Supporting Information for

Synthesis, Characterization, and Polymerization of Capped Paddlewheel Porous Cages

Meaghan M. Deegan and Eric D. Bloch*

Department of Chemistry and Biochemistry, University of Delaware, Newark, DE 19716, USA

Contents:

1. Experimental Details

1.1 General Considerations

All syntheses and manipulations were carried out using standard Schlenk and glovebox techniques unless otherwise specified. Anhydrous ethylene glycol was purchased from Sigma-Aldrich. Anhydrous DMA was purchased from Acros Organics and stored in a glovebox over molecular sieves prior to use. All other solvents were deoxygenated by thoroughly sparging with Ar and dried on a solvent purification system by SG Water, USA LLC. Syntheses of the H-esp ligand and the symmetric complex Mo_2(H-esp)$_2$ were carried out as previously reported[12]; an analogous approach to the synthesis of *t*-butyl functionalized ligand derivative (^{t}Bu-esp) is outlined below. Diisopropyl amine and isobutyronitrile were dried by passing through activated basic alumina prior to use. All other reagents were purchased from commercial suppliers or synthesized according to previously reported protocols.

1.2 Physical Methods

Gas Adsorption Measurements

Low-pressure gas adsorption measurements were obtained on a Micromeritics Tristar II PLUS or a Micromeritics 3Flex. High-pressure methane adsorption was measured with a PCT Pro-2000 Volumetric Adsorption Analyzer. Following solvent exchange, solvent was decanted and residual solvent was removed *in vacuo* to obtain cage materials as free flowing powders. Samples were then activated under vacuum at a temperature optimized for each material (see below) using a Micromeritics 3Flex Degas Station over two days.

IR Spectroscopy

IR spectra were obtained on a Bruker ALPHA II ATR-IR spectrometer with OPUS data processing software. Air sensitive samples were transferred from an inert atmosphere glovebox immediately prior to measurements, which were carried out in air.

Thermogravimetric Analysis

Thermogravimetric analysis measurements were obtained using a TA Q5000 SA under N_2 flow. Samples were transferred from an inert atmosphere glovebox and loaded onto a tared aluminum pan immediately prior to initiating measurements. During the course of the measurements, samples were heated from room temperature to 600 °C at a rate of 2 °C per minute.

UV-Visible Spectroscopy

UV-Visible Spectra were collected using an Avantes AvaSpec-ULS2048CL-EVO (CMOS) spectrometer in 1 cm glass cuvettes with a teflon-sealed screw cap.

---

(1) Pakula, R. J.; Martinez, A. M.; Noten, E. A.; Harris, C. F.; Berry, J. F. New chromium, molybdenum, and cobalt complexes of the chelating esp ligand. *Polyhedron* **2019**, *161*, 93-103.
(2) Powers, D. C.; Ritter, T. Bimetallic Pd(III) complexes in palladium-catalysed carbon-heteroatom bond formation. *Nat. Chem.* **2009**, *1*, 302-309.

NMR Spectroscopy

NMR spectra (^{1}H, ^{13}C, and DOSY) were collected at room temperature (25 °C) on Bruker 400 MHz spectrometers. ^{1}H and ^{13}C chemical shifts are reported in ppm, relative to tetramethylsilane using residual resonances from solvent as internal standards.

SEM Images

Scanning Electron Microscope images were collected using an SEM/FIB Auriga 60 housed in the Advanced Materials Characterization Laboratory at the University of Delaware.

1.3 Experimental Procedures

Ligand Synthesis

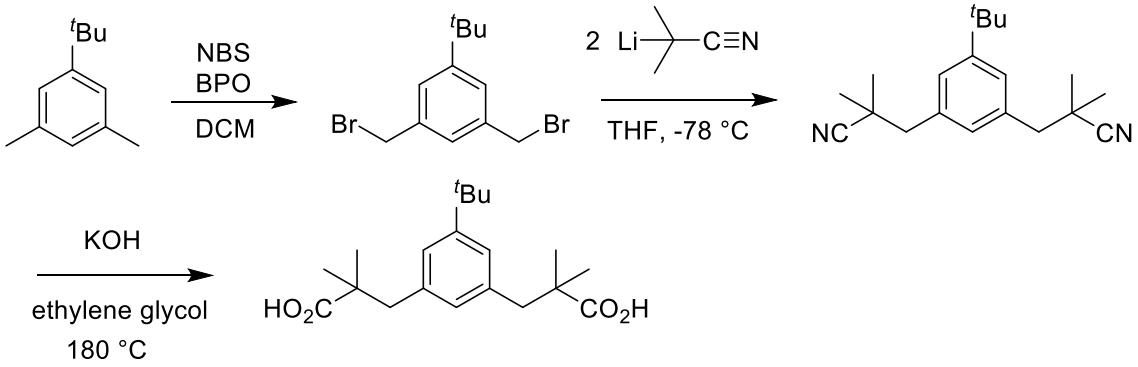

1,3-Bis(2-methyl-2-cyanopropyl)-5-*tert*-butyl-benzene: A stirred solution of diisopropyl amine (4.49 mL, 32 mmol, 2.05 equiv) in THF (100 mL) was cooled to -78 °C and *n*-BuLi (20 mL, 1.6 M in hexanes, 32 mmol, 2.05 equiv) was added. The solution was stirred at that temperature for 20 min then isobutyronitrile (2.9 mL, 32.3 mmol, 2.05 equiv) was added and the reaction was stirred for an additional 40 min. Next, 1,3-bis(bromomethyl)-5-*tert*-butyl benzene (5 g, 15.6 mmol, 1 equiv) was added to the reaction mixture and the solution was allowed to warm to room temperature. After warming, the reaction was quenched by adding water (10 mL), extracted into ethyl acetate (2 x 100 mL), and then washed with brine (1 x 50 mL). The combined organic layers were dried over $MgSO_4$ and then filtered through silica. Following solvent removal the crude material was isolated as an off-white solid. Addition of hexanes to the crude material followed by storage in the freezer overnight yielded the purified product as a white solid following filtration (3.19 g; 69 %). ^{1}H NMR ($CDCl_3$, 400 MHz): 7.23 (2H, d, J = 2 Hz), 6.97 (1H, t, J = 2 Hz), 2.81 (4H, s), 1.35 (12H, s), 1.33 (9H, s). $^{13}C\{^{1}H\}$ NMR ($CDCl_3$, 101 MHz): 151.5, 135.5, 129.3, 126.5, 124.9, 46.9, 34.7, 33.8, 31.4, 26.7. IR (solid): ν_{CN} = 2227 cm^{-1}.

^{t}Bu-esp: The ligand precursor (3.869 g, 13.1 mmol, 1 equiv) and KOH (3.71 g, 5 equiv) were combined with anhydrous ethylene glycol (20 mL) in a round bottom flask fitted with a reflux condensor and heated to 180 °C overnight under a positive N_2 flow overnight. After cooling to room temperature, a 1:1 $CHCl_3/H_2O$ mixture was added (100 mL) and the water layer was acidified with 6 M HCl (pH ~ 1). The aqueous and organic layers were separated and the aqueous fraction was extracted with EtOAc (2 x 50 mL). The combined organic layers were washed with brine (50

mL) and then dried over $MgSO_4$. The crude product was isolated as an off-white solid following solvent removal at reduced pressure. Addition of hexanes to the crude product followed by storage in the freezer overnight yielded the purified product as a white solid following filtration (4.042 g, 92 %). ^{1}H NMR ($CDCl_3$, 400 MHz): 7.00 (2H, d, J = 2 Hz), 6.80 (1H, t, J = 2 Hz), 2.83 (4H, s), 1.29 (9H, s), 1.17 (12H, s). $^{13}C\{^1H\}$ NMR ($CDCl_3$, 101 MHz): 184.1, 150.4, 136.9, 128.6, 125.9, 46.5, 43.7, 34.5, 31.5, 24.6. IR (solid): $\nu_{C=O}$ = 1688 cm^{-1}.

^{t}Bu-espLi$_2$: A solution of ^{t}Bu-esp in THF (50 mL) was cooled to -78 °C. A solution of *n*-BuLi (1.6 M in hexanes, 2 equiv) was added and the reaction was stirred at -78 °C for 1 h and then at room temperature for an additional hour. After stirring was complete, the solvent was removed *in vacuo*, yielding the desired product as an off-white solid. This material was used directly for metallations without additional purification. IR (solid): $\nu_{C=O}$ = 1560 cm^{-1}.

Cage Synthesis:

H-esp cage, Mo$_{12}$(btc)$_4$(H-esp)$_6$: A solution of $[Mo_2(OAc)_2(MeCN)_6][BF_4]_2$ (236 mg, 0.32 mmol) in DMA (6 mL) was added to a suspension of Li$_2$-esp (117 mg, 0.40 mmol) in DMA (6 mL) in a 20 mL scintillation vial, which rapidly resulted in a color change from pink-orange to yellow and generated a homogenous solution. Subsequently, trimesic acid (45 mg, 0.21 mmol) and dimethylformamidium triflate (40 mg) were dissolved in DMA and then added to the reaction mixture once fully homogenized. The combined mixture was heated at 95 °C overnight, yielding a dark red solution. After cooling to room temperature, MeOH was added (~3:1 MeOH/DMA), resulting in the precipitation of an orange-red solid. Following centrifugation, the solvent was decanted and the solid was washed with MeOH over the course of three days, with the solvent exchanged for neat MeOH once daily.

^{t}Bu-esp Cage, Mo$_{12}$(btc)$_4$(^{t}Bu-esp)$_6$: Stock solutions of each of the reaction components were prepared in DMA as follows: ^{t}Bu-espLi$_2$ (113 mg, 0.32 mmol) in 10 mL, $[Mo_2(OAc)_2(MeCN)_6][BF_4]_2$ (197 mg, 0.27 mmol) in 10 mL, trimesic acid (38 mg, 0.18 mmol) in 5 mL, and dimethylformamidium triflate (35 mg) in 5 mL. The $[Mo(OAc)_2(MeCN)_6][BF_4]_2$ was added to 10 separate 4 mL scintillation vials (1 mL each) and the ^{t}Bu-esp-Li$_2$ stock solution was added (1 mL). The solutions of trimesic acid and dimethylformamidium triflate were combined and an additional 1 mL of this solution was added to each 4 mL vial. The solutions were heated at 95 °C overnight and then cooled to room temperature, yielding red solutions. These were combined and then diluted with MeOH (~3:1 MeOH/DMA), resulting in the precipitation of the desired product as an orange-red solid. Following centrifugation, the solvent was decanted and the solid was washed with MeOH over the course of three days, with the solvent exchanged for neat MeOH once daily. We note that the same reaction can be carried out instead in a 20 mL scintillation vial at similar concentrations. In our hands this sometimes led to the undesirable formation of an insoluble material after heating, we thus preferred to prepare this material iteratively in smaller, 4 mL vials.

DABCO polymerization: A solution of the H-esp cage, Mo$_{12}$(btc)$_4$(H-esp)$_6$, in DMA was generated as described above. After cooling to room temperature, DABCO (74.6 mg, approximately 4 equiv per cage) was added to the reaction solution, which was then heated at 95

°C for a second night. After heating, the DABCO-pillared material precipitated from solution as an amorphous solid. This solid was washed with THF over 3 days with solvent exchanged once daily. The solid was vacuum activated at 200 °C over 2 days, washed with THF to remove sublimed DABCO and then activated a second time at 200 °C.

2. NMR Spectra

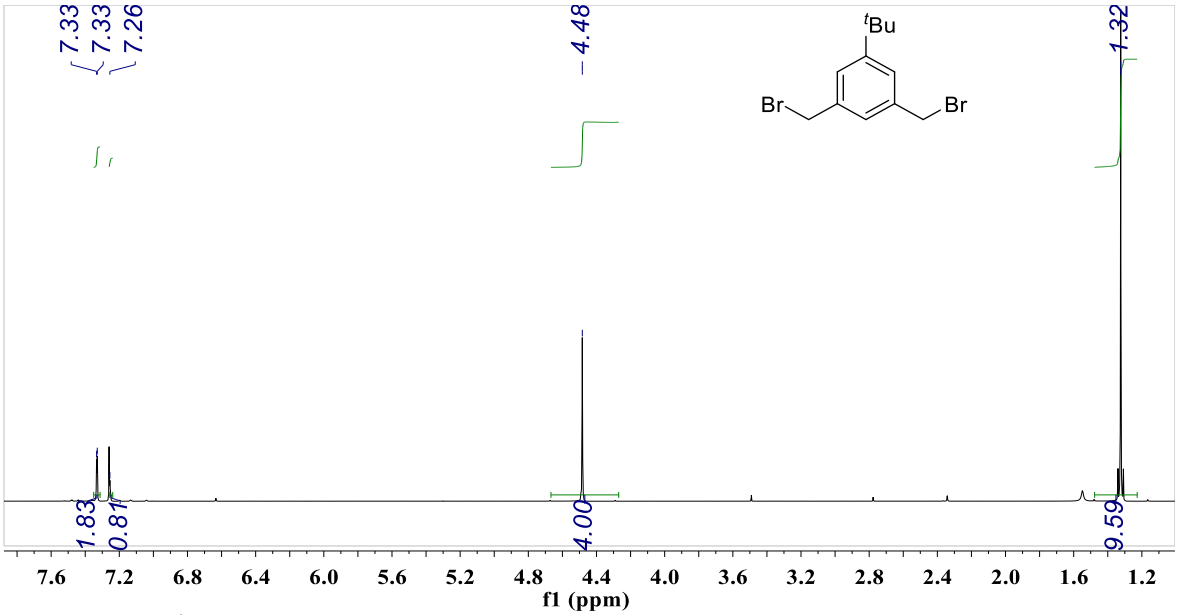

Figure S2.1. ^{1}H NMR spectrum (400 MHz) of 1,3-bis(bromomethyl)-5-*tert*-butyl-benzene in $CDCl_3$ at room temperature.

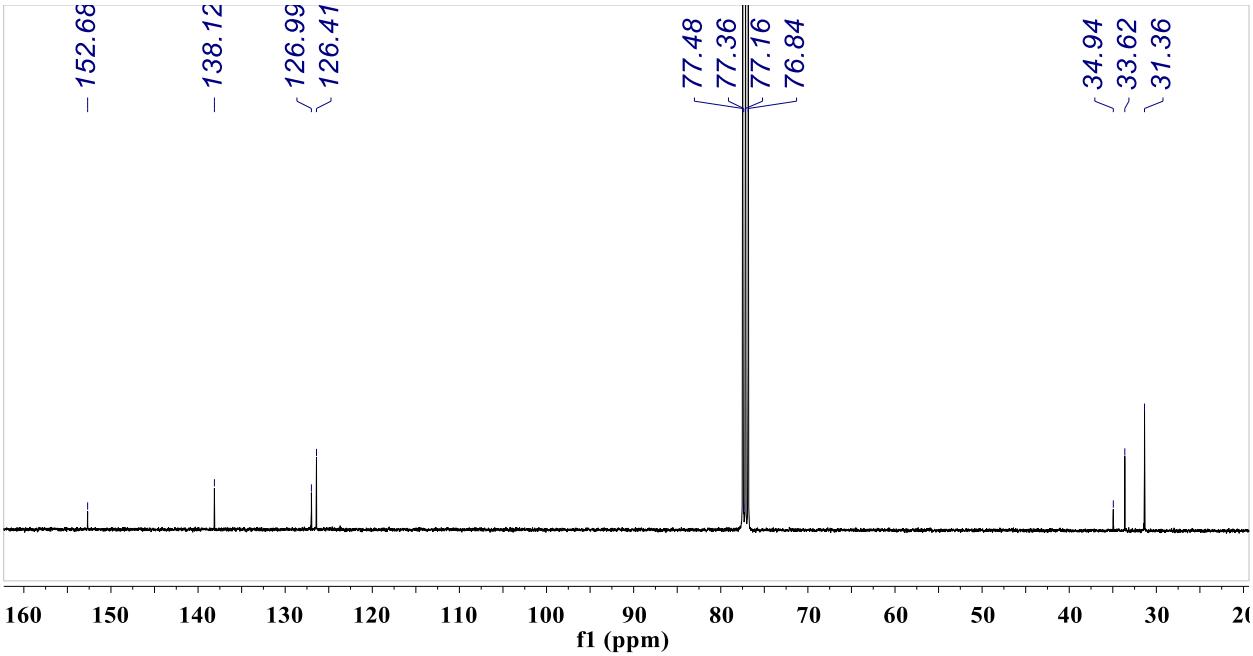

Figure S2.2. ^{13}C NMR spectrum (101 MHz) of 1,3-bis(bromomethyl)-5-*tert*-butyl-benzene in $CDCl_3$ at room temperature

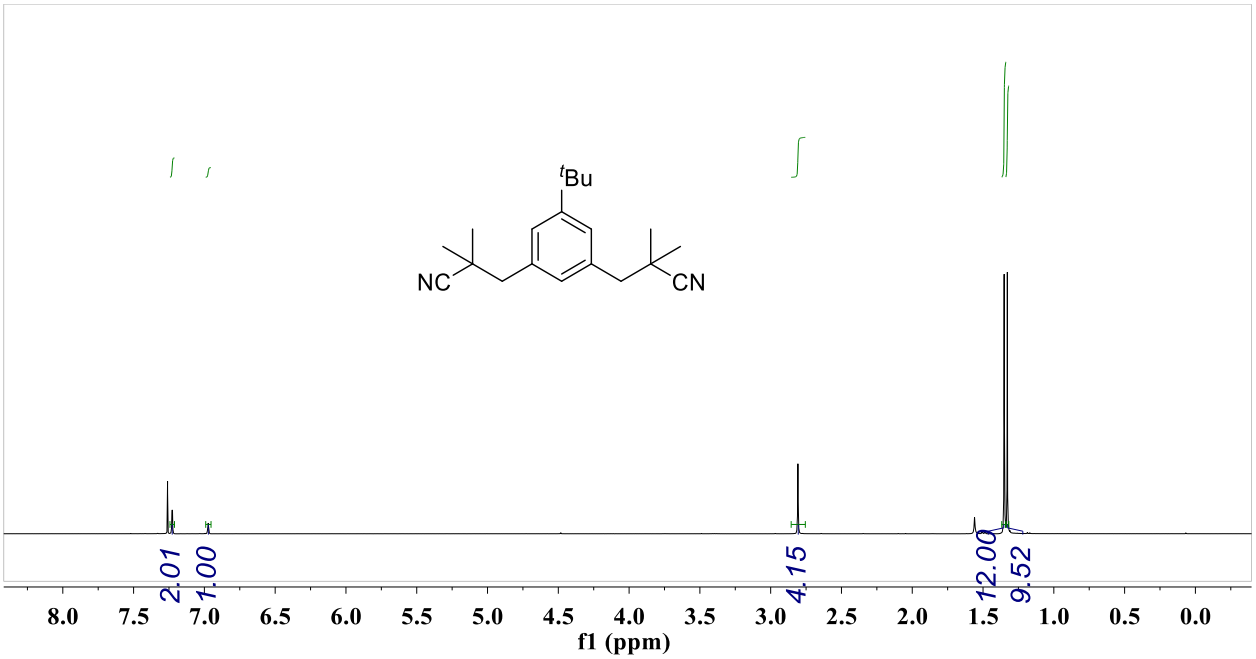

Figure S2.3. ^{1}H NMR spectrum (400 MHz) of 1,3-bis(2-methyl-2-cyanopropyl)-5-*tert*-butyl-benzene in $CDCl_3$ at room temperature.

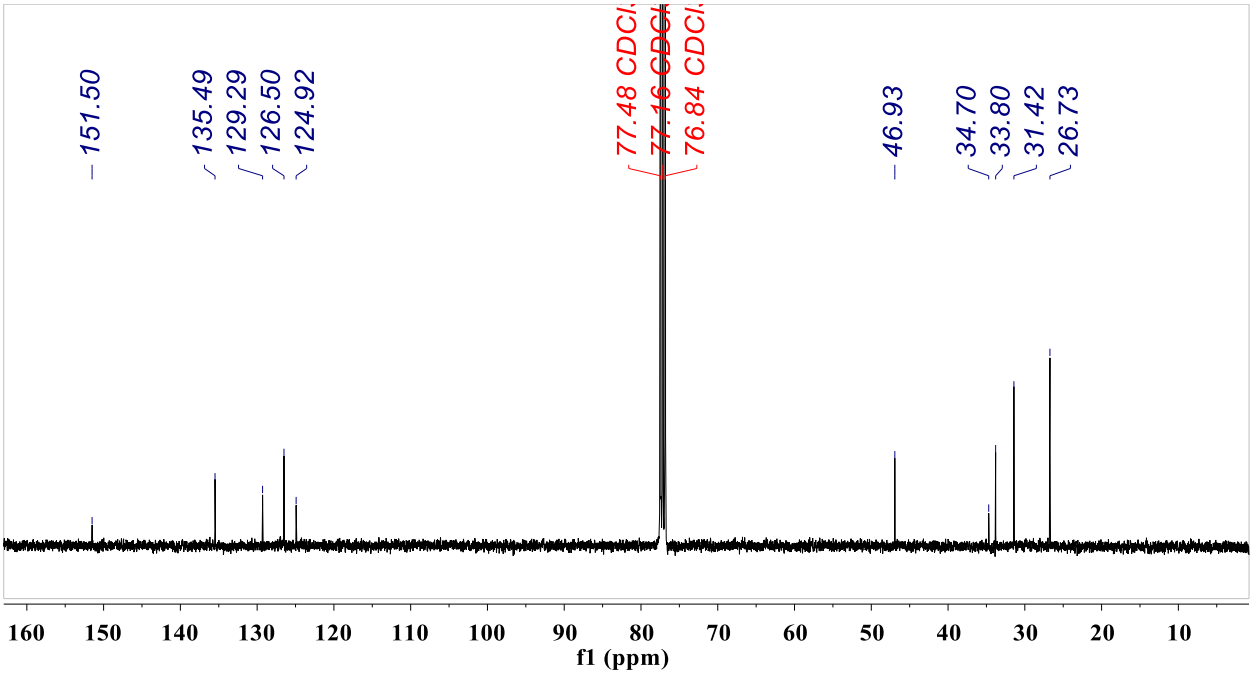

Figure S2.4. ^{13}C NMR spectrum (101 MHz) of 1,3-bis(2-methyl-2-cyanopropyl)-5-*tert*-butyl-benzene in $CDCl_3$ at room temperature.

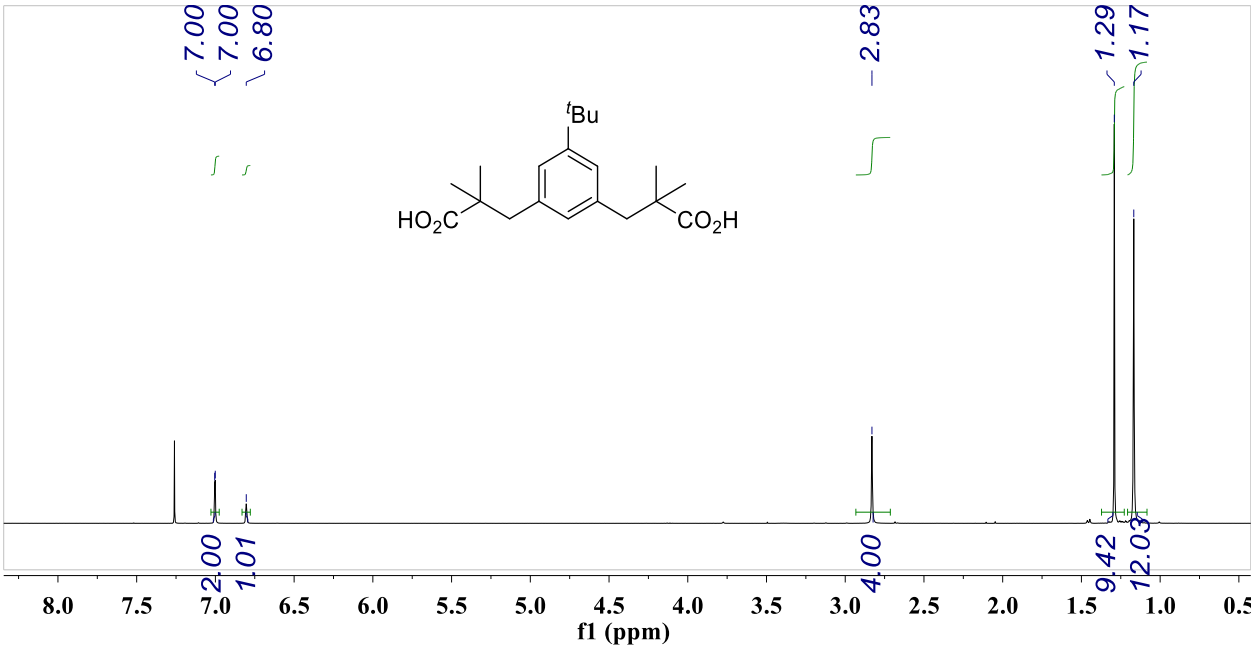

Figure S2.5. ^{1}H NMR spectrum (400 MHz) of *t*Bu-esp in $CDCl_3$ at room temperature.

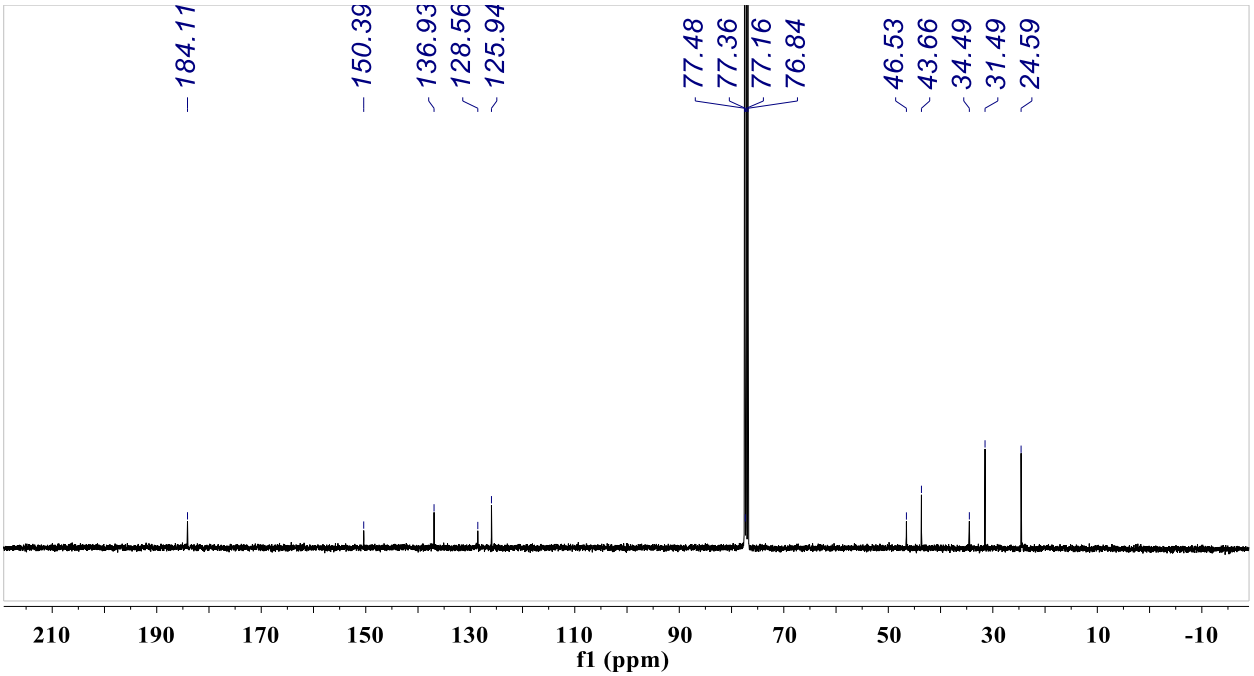

Figure S2.6. ^{13}C NMR spectrum (101 MHz) of *t*Bu-esp in $CDCl_3$ at room temperature.

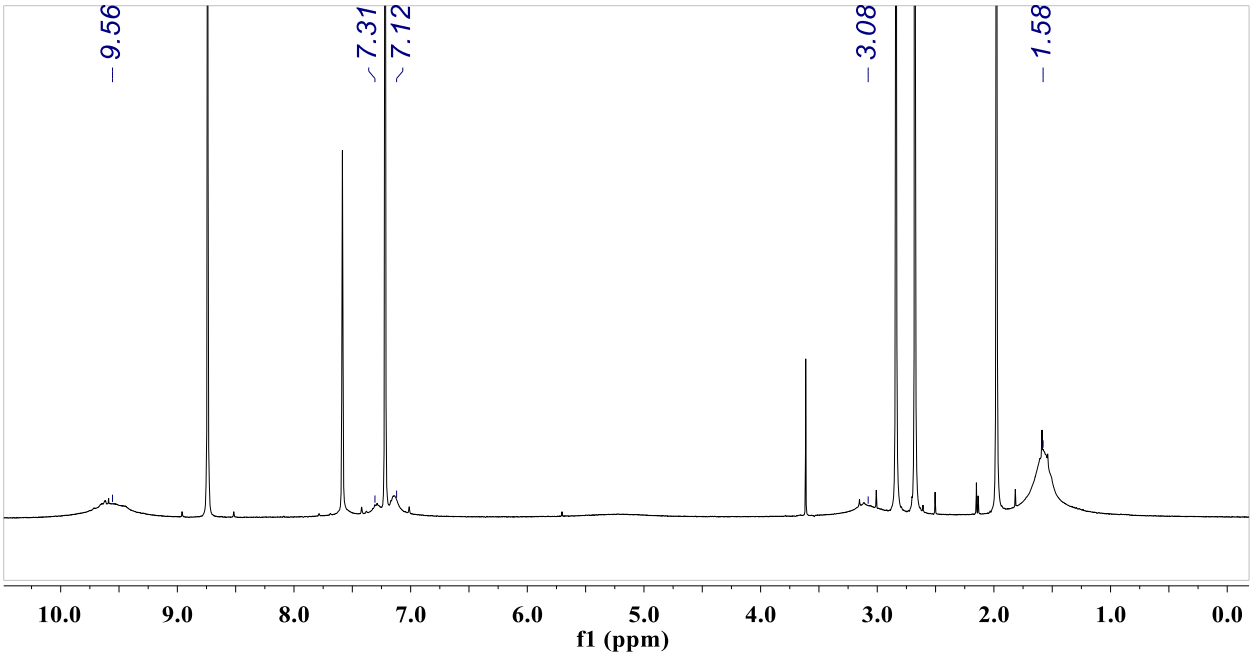

Figure S2.7. ^{1}H NMR spectrum (400 MHz) of the as synthesized H-esp cage, $Mo_{12}(btc)_4(H\text{-}esp)_6$ in pyridine-d_5. In addition to the broad peaks associated with the cage and the NMR solvent peaks, resonances associated with the synthetic solvents (DMA and MeOH) are apparent.

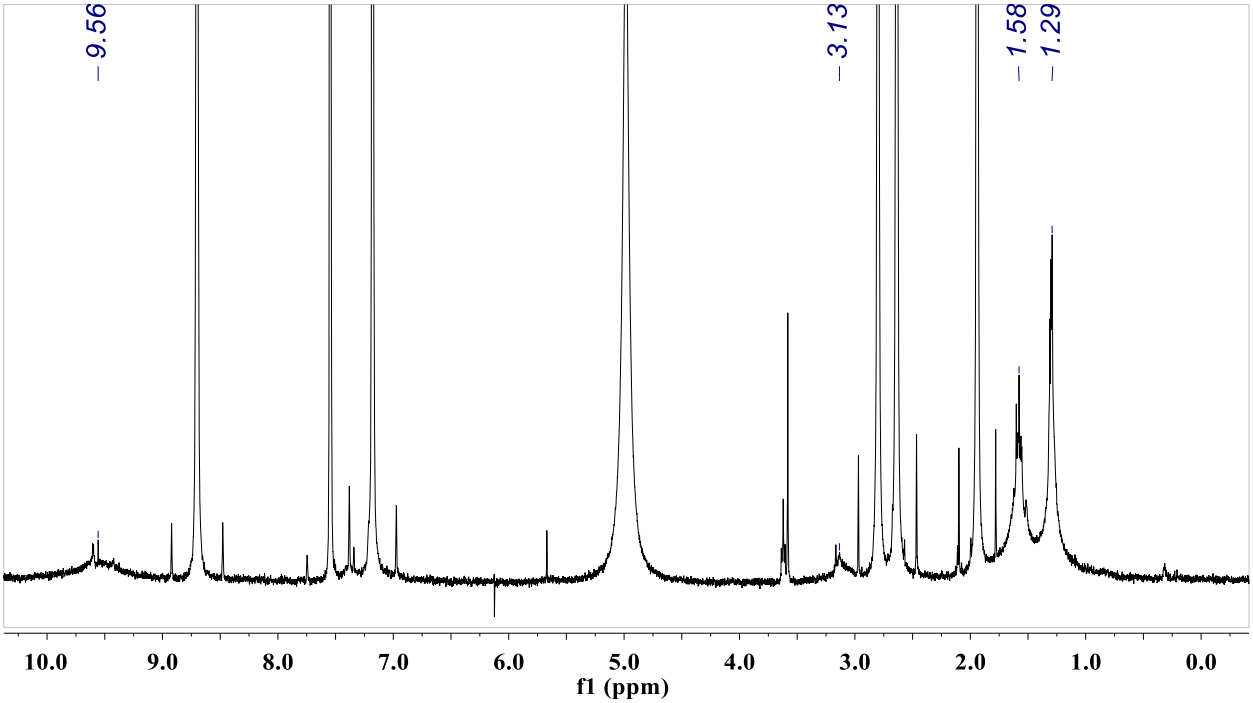

Figure S2.8. ^{1}H NMR spectrum (400 MHz) of the as synthesized ^{t}Bu-esp cage, $Mo_{12}(btc)_4(^{t}Bu\text{-}esp)_6$ in pyridine-d_5. In addition to the broad peaks associated with the cage and the NMR solvent peaks, resonances associated with the synthetic solvents (DMA and MeOH) are apparent. Broad esp-ligand aromatic resonances are overlapping with pyridine resonances and are not readily observed in the product spectrum.

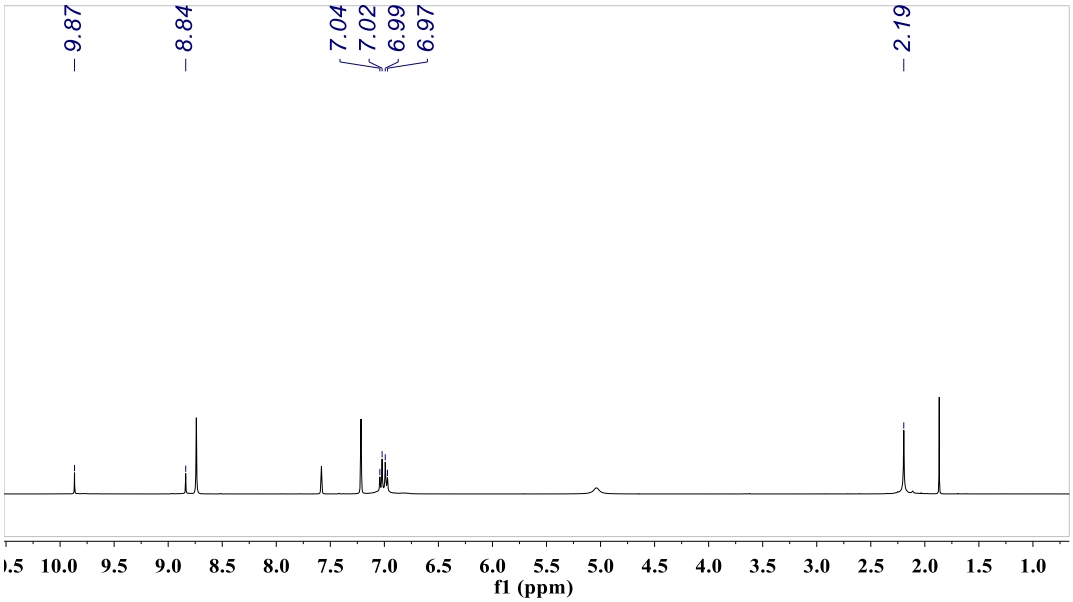

Figure S2.9. ^{1}H NMR spectrum (400 MHz) of $Mo_{12}(btc)_4(DTolF)_{12}$ in pyridine-d_5. Peaks associated with the MeOH exchange solvent are apparent in the spectrum.

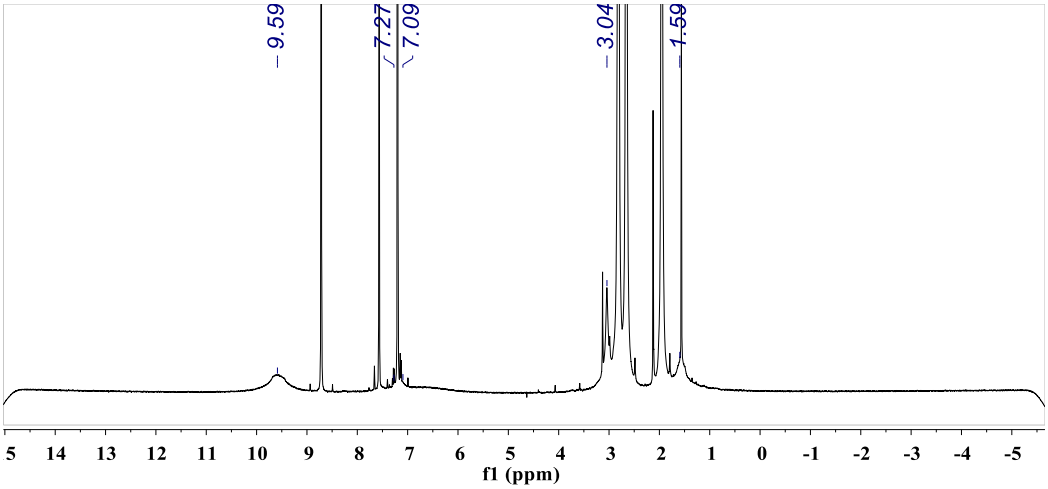

Figure S2.10. ^{1}H NMR spectrum (400 MHz) of the initially precipitated DABCO polymer, which was depolymerized and dissolved in pyridine-d_5. We note that extensive washing and/or activation of the polymer to remove residual solvent and ligand impurities significantly reduced the solubility of the material. Resonances associated with DABCO directly overlap with residual DMA (2.65 ppm).

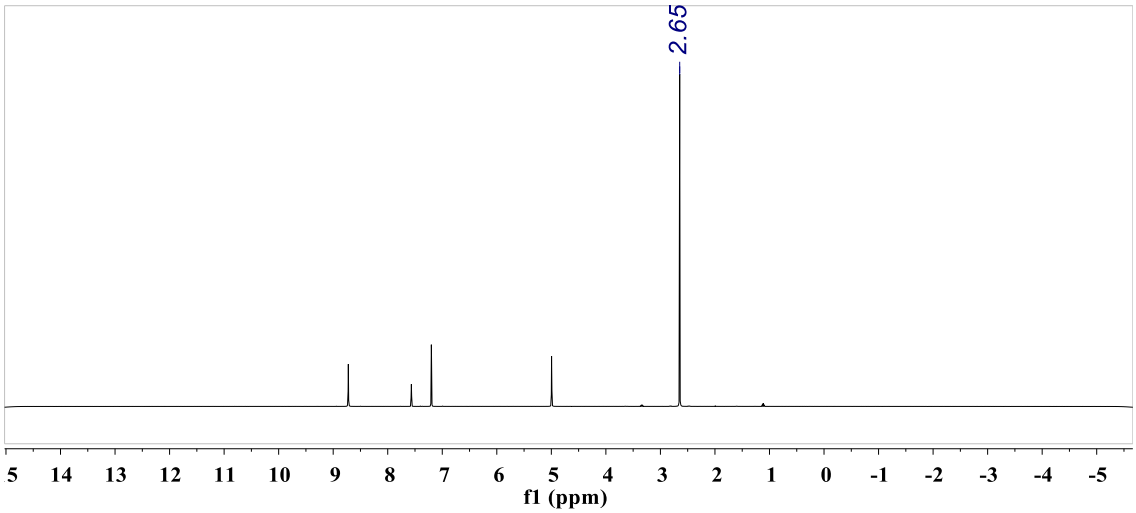

Figure S2.11. ^{1}H NMR specrtum (400 MHz) of DABCO in pyridine-d_5.

DOSY Experiments

$Mo_{12}(btc)_4(DTolF)_{12}$[3]

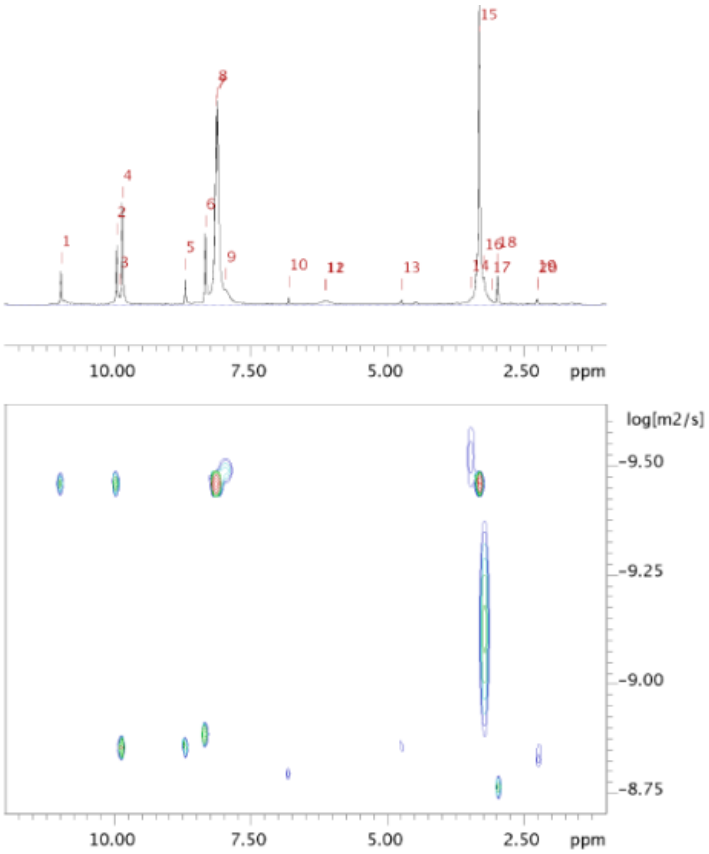

Figure S2.12. Plotted DOSY data (400 MHz) for $Mo_{12}(btc)_4(DTolF)_{12}$ collected in pyridine-d_5 at room temperature.

Table S2.1. DOSY data for $Mo_{12}(btc)_4(DTolF)_{12}$.

Peak Number	Chemical Shift (ppm)	Diffusion rate (m^2/s)	Radius[a] (Å)
1	10.99	3.48×10^{-10}	7.12
2	9.96	3.49×10^{-10}	7.10
7	8.15	3.39×10^{-10}	7.31
8	8.11	3.41×10^{-10}	7.27
15	3.32	3.48×10^{-10}	7.12
Average	--	3.45×10^{-10}	7.19

[a]Calculated using the Stokes-Einstein equation approximating the molecule as a sphere.

3 Lorzing, G. R.; Gosselin, E. J.; Lindner, B. S.; Bhattacharjee, R.; Yap, G. P. A.; Caratzoulas, S.; Bloch, E. D. Design and Synthesis of Capped-Paddlewheel-Based Porous Coordination Cages. *Chem. Commun.* **2019**, *55*, 9527-9530.

H-esp cage: $Mo_{12}(btc)_4(esp)_6$

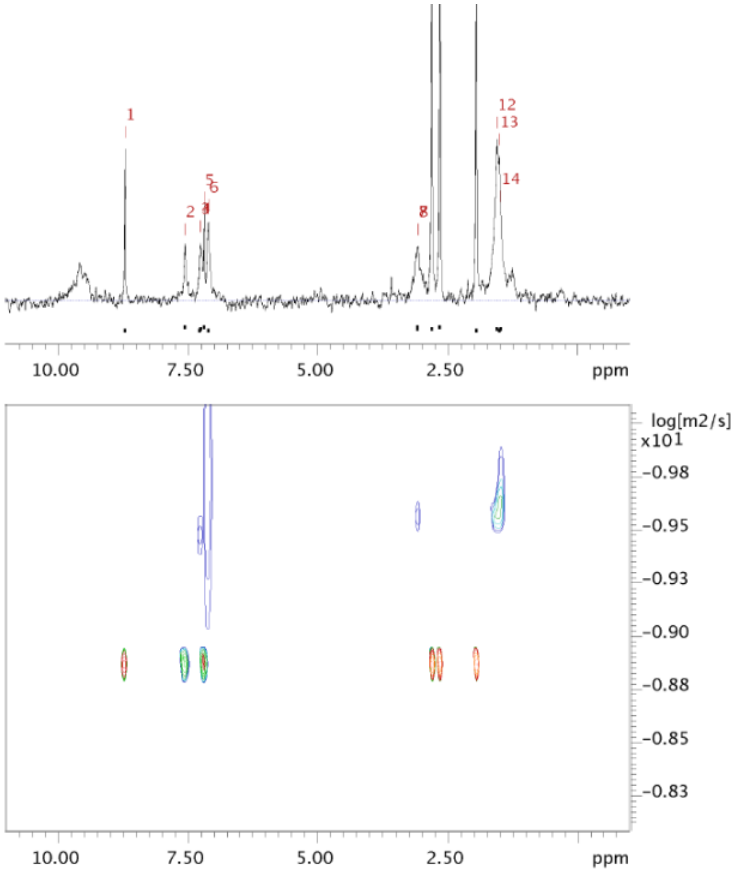

Figure S2.13. Plotted DOSY data (400 MHz) for $Mo_{12}(btc)_4(H\text{-}esp)_6$ collected in pyridine-d_5 at room temperature.

Table S2.2. DOSY data for $Mo_{12}(btc)_4(H\text{-}esp)_6$. Multiple positions are noted for some peaks because of the broadness of the cage resonances.

Peak Number	Chemical Shift (ppm)	Diffusion rate (m^2/s)	Radius[a] (Å)
4	7.25	3.02×10^{-10}	8.21
6	7.10	1.89×10^{-10}	13.1
7	3.08	3.00×10^{-10}	8.26
8	3.07	1.66×10^{-10}	14.9
12	1.55	2.85×10^{-10}	8.70
13	1.50	2.13×10^{-10}	11.6
14	1.48	1.71×10^{-10}	14.5
Average	--	2.32×10^{-10}	10.7

[a]Calculated using the Stokes-Einstein equation approximating the molecule as a sphere.

^{t}Bu-esp cage: $Mo_{12}(btc)_4(^{t}Bu\text{-}esp)_6$

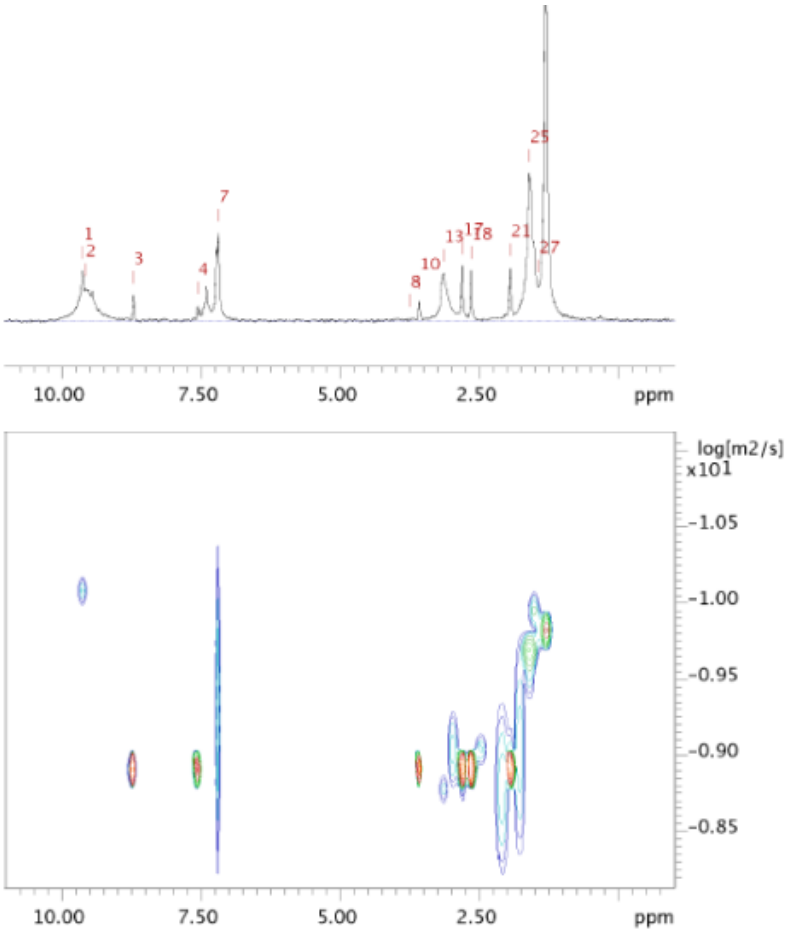

Figure S2.14. Plotted DOSY data (400 MHz) for $Mo_{12}(btc)_4(^{t}Bu\text{-}esp)_6$ collected in pyridine-d_5 at room temperature.

Table S2.3. DOSY data for $Mo_{12}(btc)_4(^{t}Bu\text{-}esp)_6$. Multiple positions are noted for some peaks because of the broadness of the cage resonances.

Peak Number	Chemical Shift (ppm)	Diffusion rate (m^2/s)	Radius[a] (Å)
1	9.61	8.07×10^{-11}	30.7
2	9.57	7.16×10^{-11}	34.6
7	7.18	5.54×10^{-10}	4.48
14	3.11	6.37×10^{-11}	38.9
25	1.61	1.91×10^{-10}	13.0
26	1.53	9.79×10^{-11}	25.3
27	1.44	1.33×10^{-10}	18.6
28	1.31	1.34×10^{-10}	18.5
Average[b]	--	1.10×10^{-10}	22.5

[a]Calculated using the Stokes-Einstein equation approximating the molecule as a sphere.
[b]Omits peak 7, which gives an anomalous, low value. Analysis at this position may be complicated by overlapping solvent.

3. IR Spectra

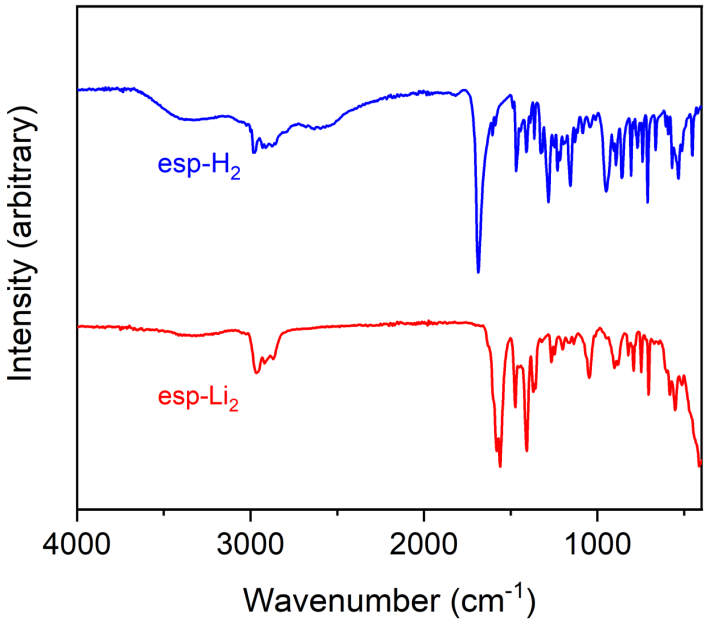

Figure S3.1. IR spectra of the as synthesized H-esp ligand (top, blue) and the ligand following deprotonation with *n*-BuLi (bottom, red).

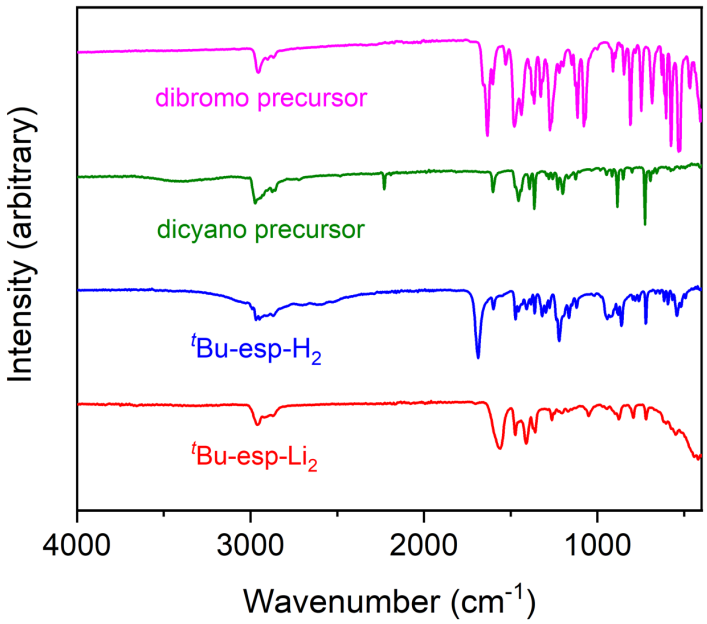

Figure S3.2. IR spectra of the ^{t}Bu-esp ligand (blue), its lithium salt (^{t}Bu-espLi$_2$; red), and its synthesized precursors (pink, green).

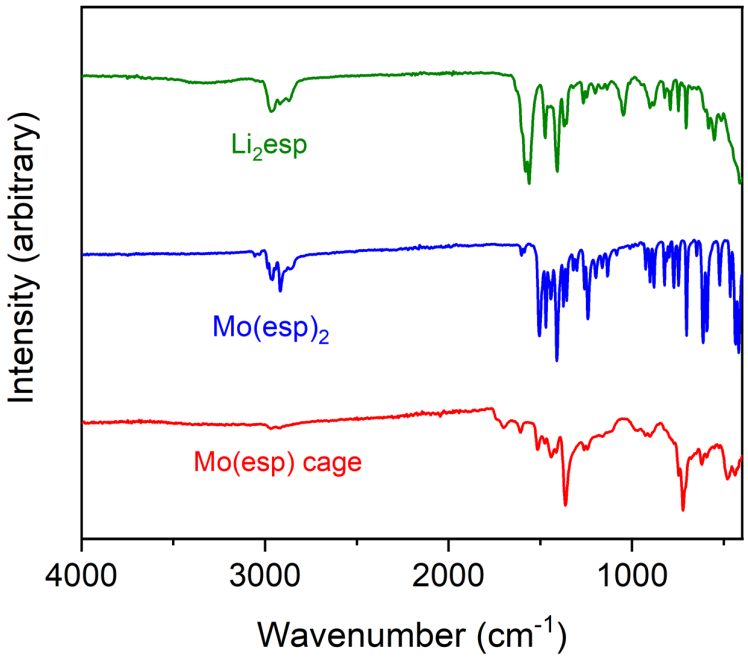

Figure S3.3. IR spectra of the lithiated esp ligand (green), the symmetric molybdenum complex $Mo(esp)_2$ (blue), and the H-esp cage, $Mo_{12}(btc)_4(H\text{-}esp)_6$ (red). Vertical lines highlight Mo-bound trimesic acid C=O stretches (left) and Mo-bound esp stretches (right).

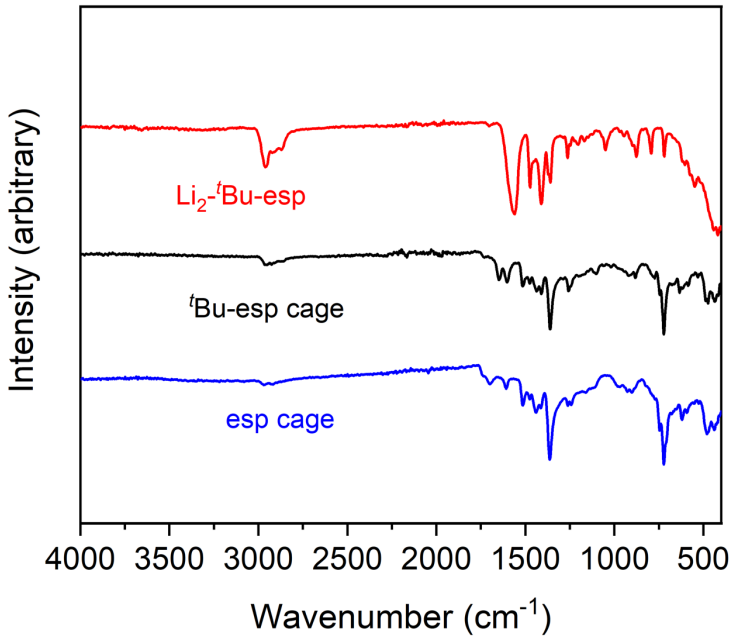

Figure S3.4. IR spectra of the lithiated ^{t}Bu-esp ligand (red), the Mo(^{t}Bu-esp) cage, $Mo_{12}(btc)_4(^t\text{Bu-esp})_4$ (black), and the Mo(H-esp) cage $Mo_{12}(btc)_4(H\text{-}esp)_4$ (blue).

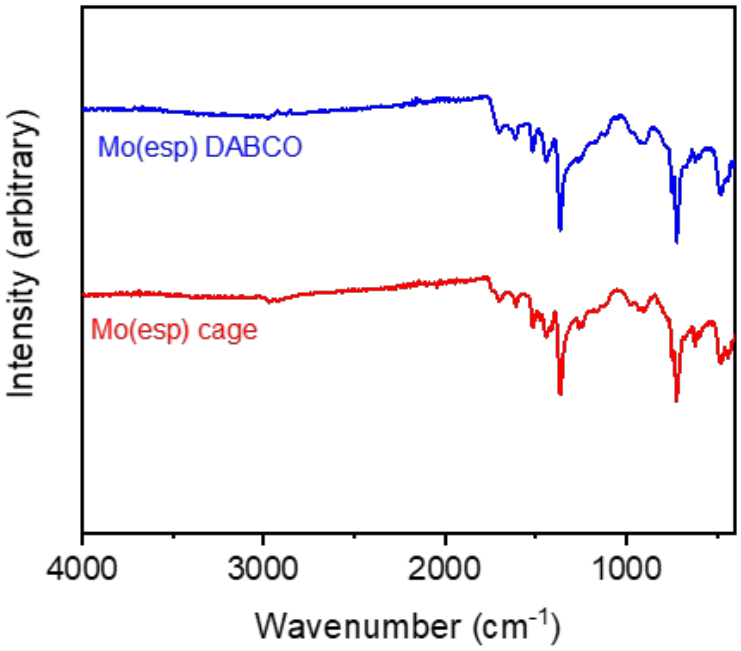

Figure S3.5. IR spectra of polymerized and activated DABCO polymer (blue) and the isolated molecular cage $Mo_{12}(btc)_4(H\text{-}esp)_4$ (red).

4. Gas Adsorption

Degas Surveys

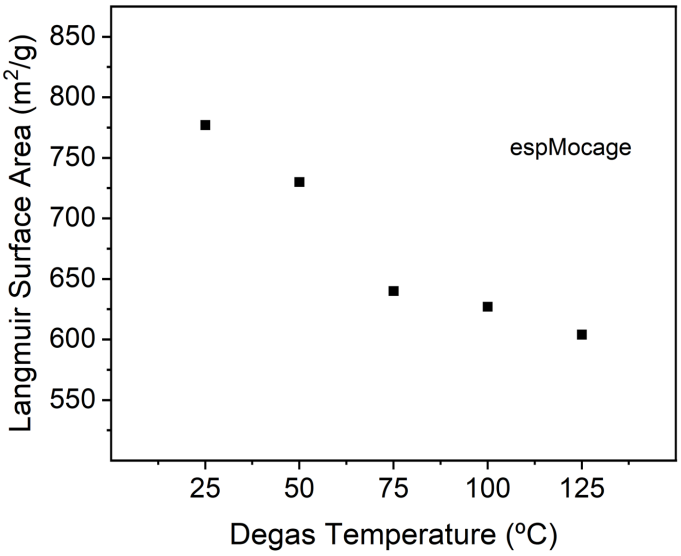

Figure S4.1. Plot showing how the surface area of the H-esp-capped cage varies as the activation temperature is increased. For each point a synthesized sample was vacuum activated at the specified temperature overnight and an adsorption isotherm was measured to determine the N_2 accessible Langmuir surface area at 77 K.

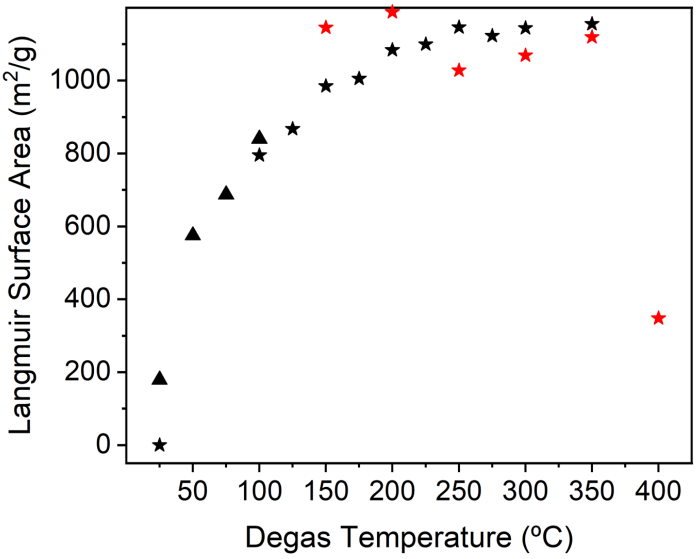

Figure S4.2. Plot showing how the surface area of the DABCO polymerized cage varies as the activation temperature is increased. Black and red symbols represent two independent samples. Stars represent N_2 accessible surface areas (77 K); triangles represent CO_2 accessible surface areas (195 K).

Full isotherms
Esp-Mo cage pyridine/MeOH N_2

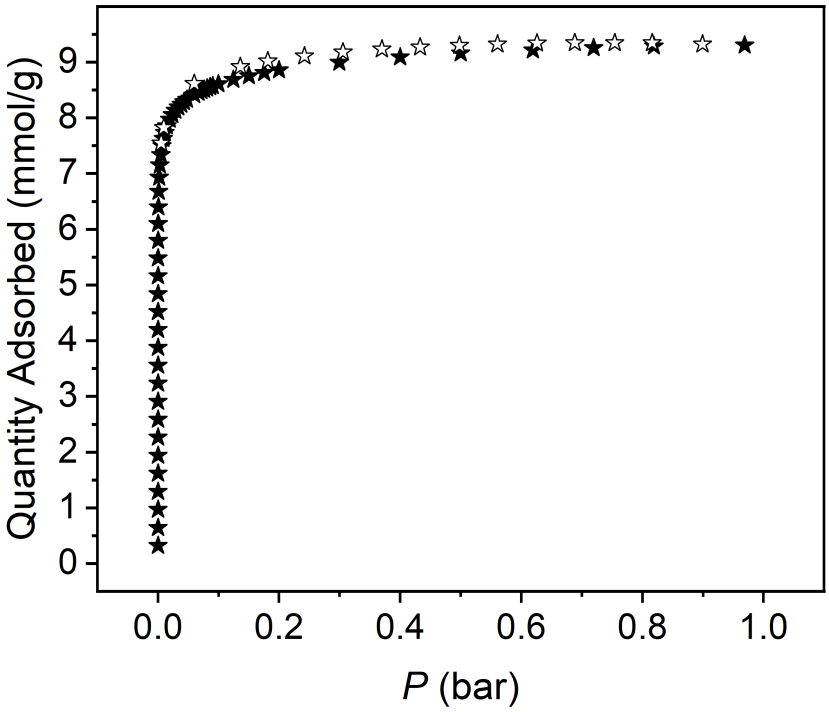

Figure S4.3. N_2 adsorption (closed stars) and desorption (open stars) measured at 77 K for the H-esp Mo cage activated under optimal conditions.

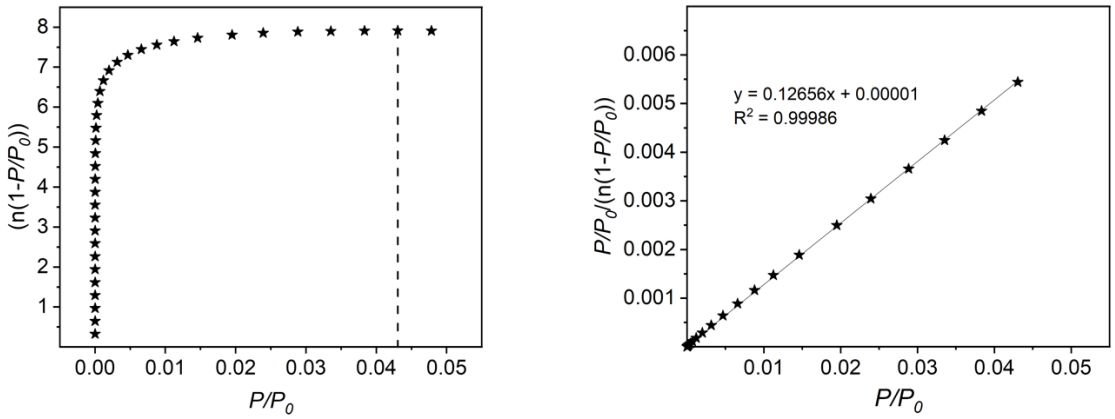

Figure S4.4. Left: Plot of n(1-P/P_0) vs. P/P_0 to determine the maximum P/P_0 used in the BET linear fit according to the first BET consistency criterion for N_2 adsorption at 77 K for the H-esp cage. Right: The slope of the best fit line for $P/P_0 < 0.044$ is 0.12656 and the y-intercept is 0.00001, which satisfies the second BET consistency criterion. This results in a measured surface area of 770 m^2/g.

Mo(esp) cage pyridine/MeOH CO_2

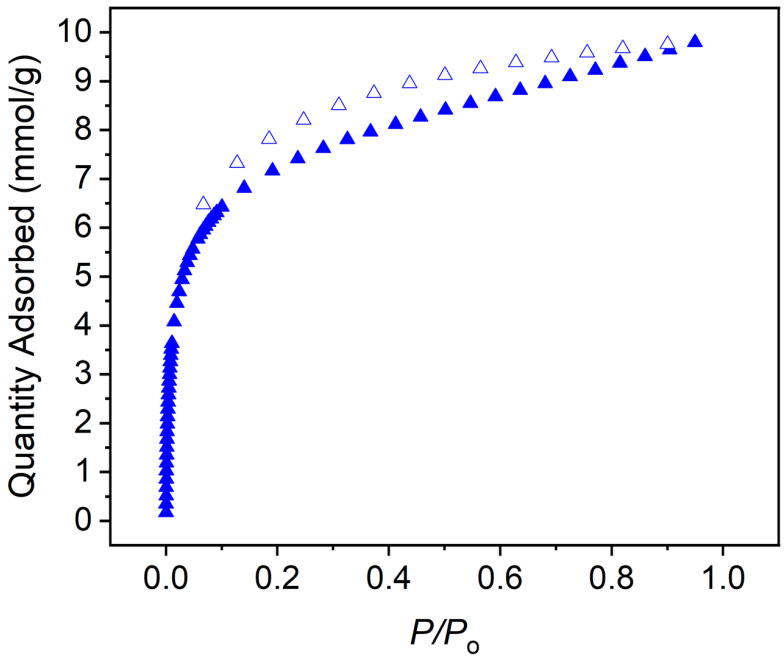

Figure S4.5. CO_2 adsorption (closed triangles) and desorption (open triangles) measured at 195 K for the H-esp cage activated under optimal conditions.

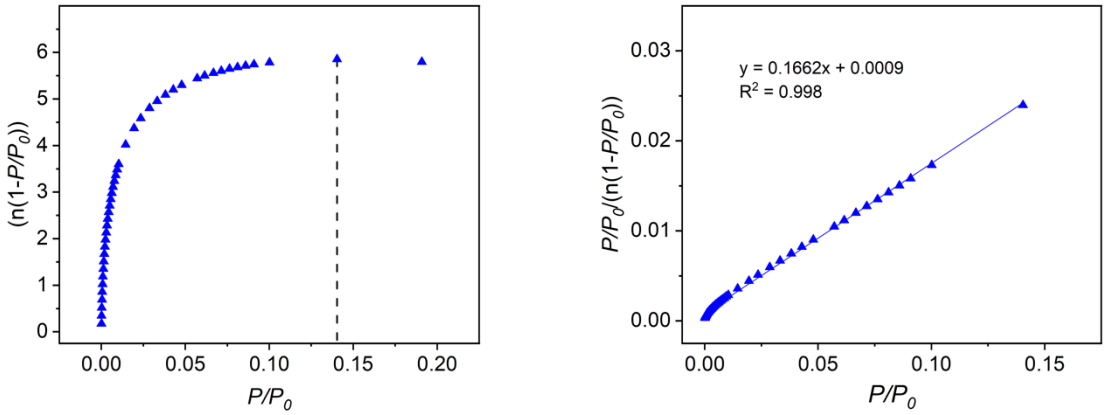

Figure S4.6. Left: Plot of n(1-P/P_0) vs. P/P_0 to determine the maximum P/P_0 used in the BET linear fit according to the first BET consistency criterion for CO_2 adsorption at 195 K for the H-esp cage. Right: The slope of the best fit line for $P/P_0 < 0.141$ is 0.1662 and the y-intercept is 0.0009, which satisfies the second BET consistency criterion. This results in a measured surface area of 616 m^2/g.

Mo(esp) cage MeOH CO_2

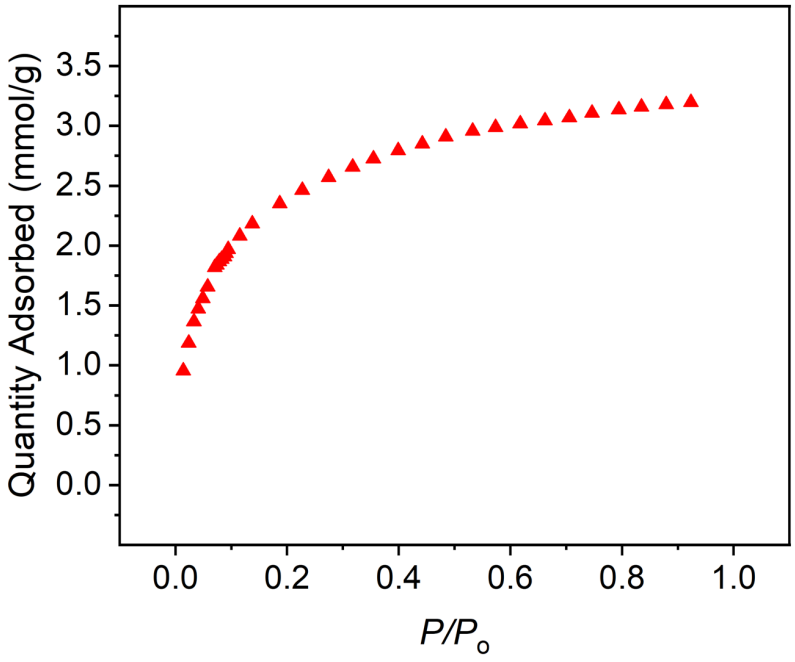

Figure S4.7. CO_2 adsorption (closed triangles) measured at 195 K for the H-esp cage precipitated from DMA with MeOH.

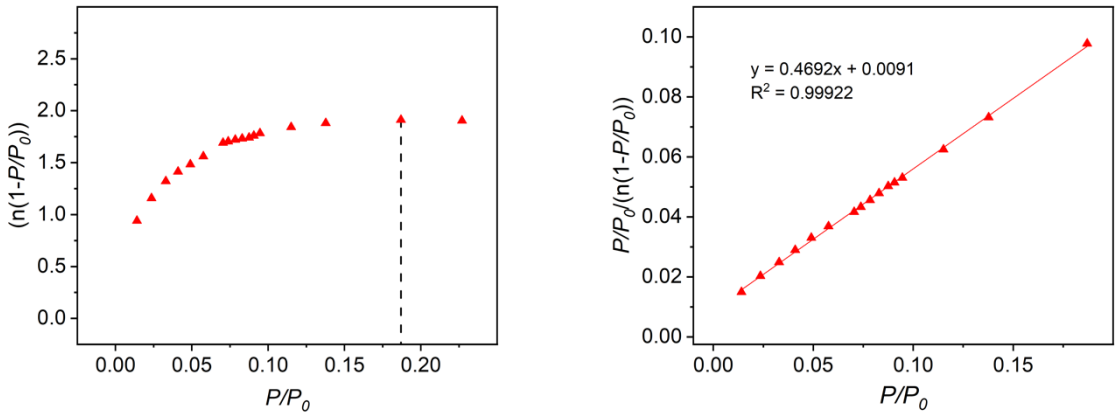

Figure S4.8. Left: Plot of n(1-P/P_0) vs. P/P_0 to determine the maximum P/P_0 used in the BET linear fit according to the first BET consistency criterion for CO_2 adsorption at 195 K for the precipitated H-esp cage. Right: The slope of the best fit line for $P/P_0 < 0.187$ is 0.4692 and the y-intercept is 0.0091, which satisfies the second BET consistency criterion. This results in a measured surface area of 218 m^2/g.

tBu-esp Mo cage pyridine MeOH N_2

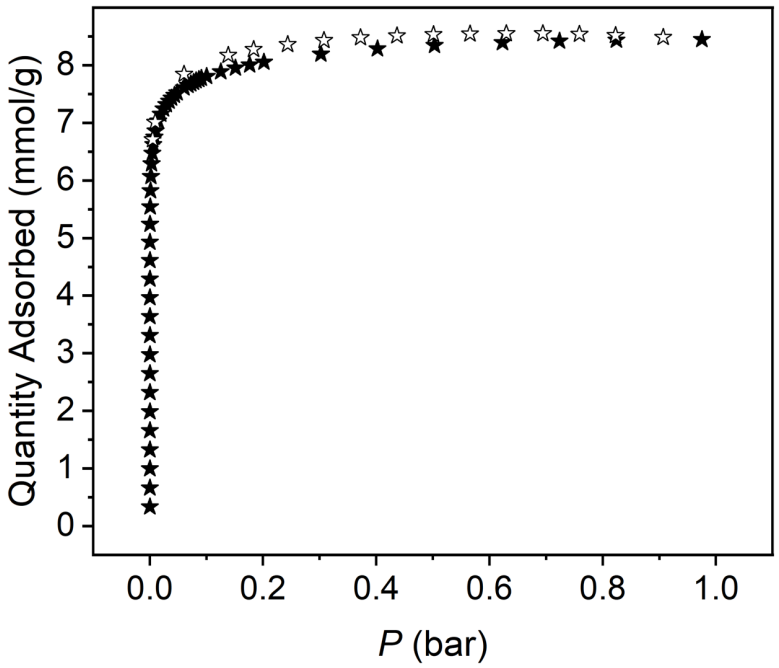

Figure S4.9. N_2 adsorption (closed stars) and desorption (open stars) measured at 77 K for the ^{t}Bu-esp cage activated under optimal conditions.

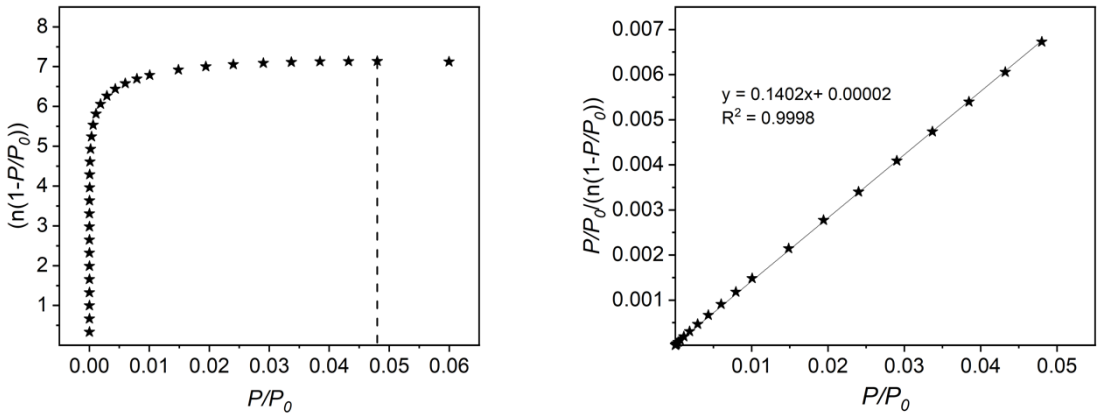

Figure S4.10. Left: Plot of n(1-P/P_0) vs. P/P_0 to determine the maximum P/P_0 used in the BET linear fit according to the first BET consistency criterion for N_2 adsorption at 77 K for the ^{t}Bu-esp cage. Right: The slope of the best fit line for $P/P_0 < 0.048$ is 0.1402 and the y-intercept is 0.00002, which satisfies the second BET consistency criterion. This results in a measured surface area of 696 m^2/g.

tBuesp Mo cage pyridine MeOH CO_2

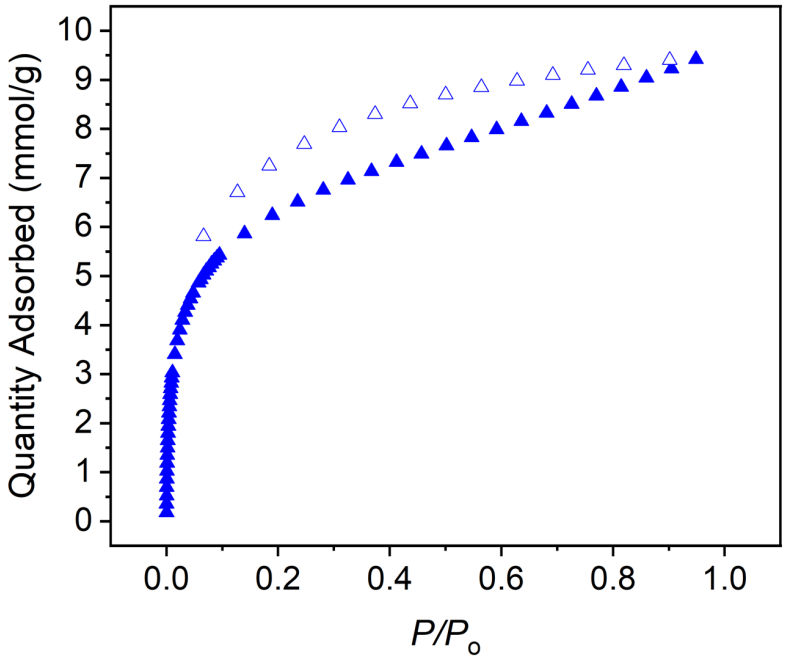

Figure S4.11. CO_2 adsorption (closed triangles) and desorption (open triangles) measured at 195 K for the ^{t}Bu-esp cage activated under optimal conditions.

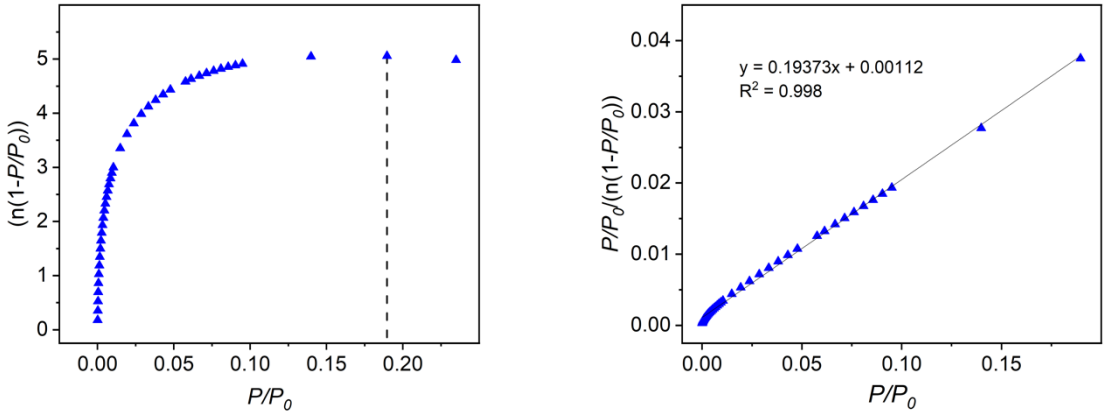

Figure S4.12. Left: Plot of n(1-P/P_0) vs. P/P_0 to determine the maximum P/P_0 used in the BET linear fit according to the first BET consistency criterion for CO_2 adsorption at 195 K for the ^{t}Bu-esp cage. Right: The slope of the best fit line for $P/P_0 < 0.190$ is 0.19373 and the y-intercept is 0.00112, which satisfies the second BET consistency criterion. This results in a measured surface area of 529 m^2/g.

tBuesp Mo cage MeOH CO_2

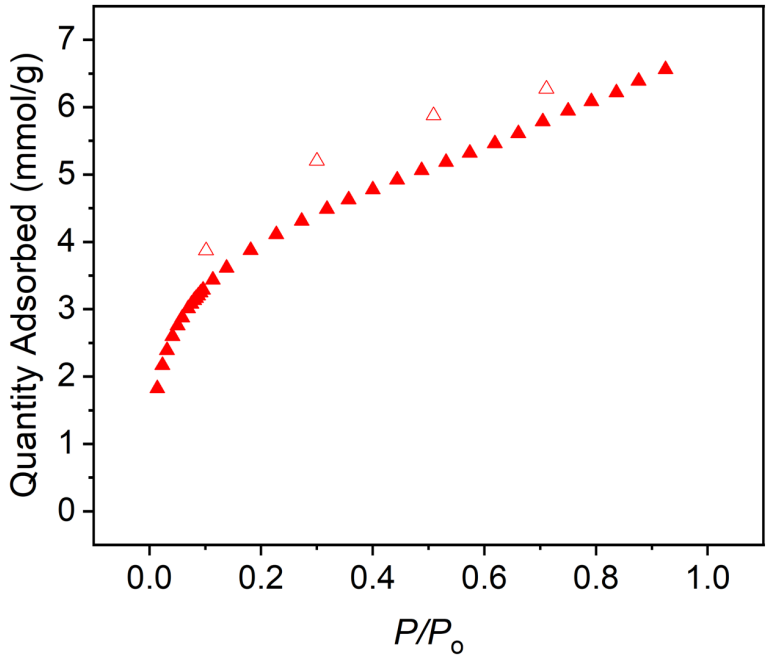

Figure S4.13. CO_2 adsorption (closed triangles) and desorption (open triangles) emeasured at 195 K for the ^{t}Bu-esp cage precipitated from DMA with MeOH.

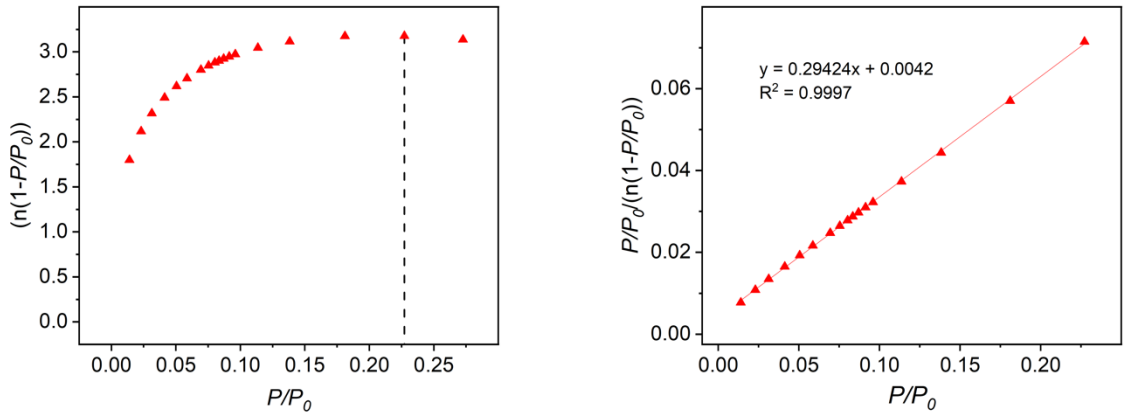

Figure S4.14. Left: Plot of n(1-P/P_0) vs. P/P_0 to determine the maximum P/P_0 used in the BET linear fit according to the first BET consistency criterion for CO_2 adsorption at 195 K for the precipitated ^{t}Bu-esp cage. Right: The slope of the best fit line for $P/P_0 < 0.228$ is 0.29424 and the y-intercept is 0.0042, which satisfies the second BET consistency criterion. This results in a measured surface area of 348 m^2/g.

DABCOMo(esp) N_2

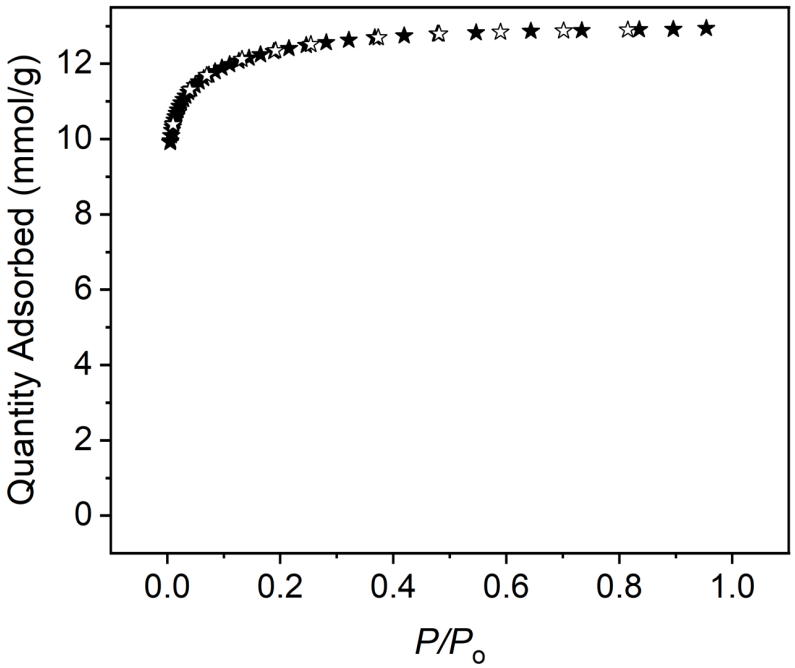

Figure S4.15. N_2 adsorption (closed stars) and desorption (open stars) measured at 77 K for the DABCO polymerized H-esp cage.

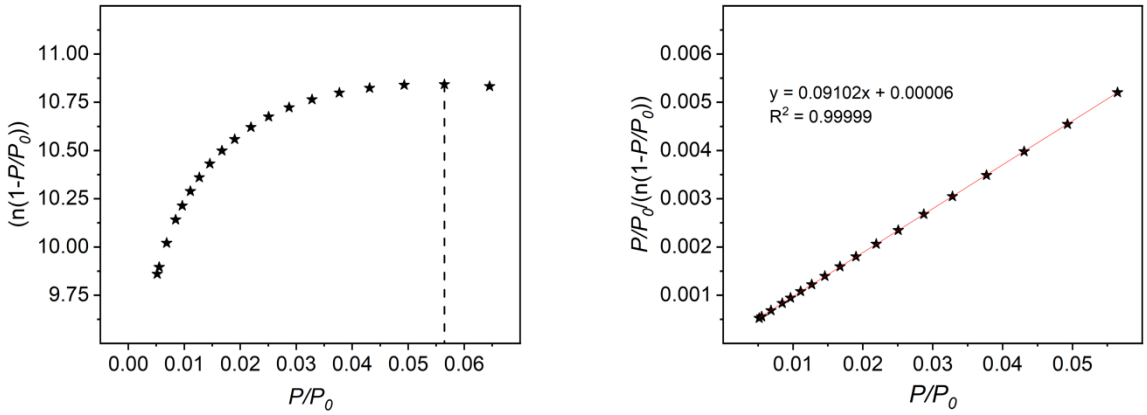

Figure S4.16. Left: Plot of n(1-P/P_0) vs. P/P_0 to determine the maximum P/P_0 used in the BET linear fit according to the first BET consistency criterion for N_2 adsorption at 77 K for the DABCO polymerized H-esp cage. Right: The slope of the best fit line for $P/P_0 < 0.057$ is 0.09102 and the y-intercept is 0.00006, which satisfies the second BET consistency criterion. This results in a measured surface area of 1072 m^2/g.

DABCOMo(esp) CO_2

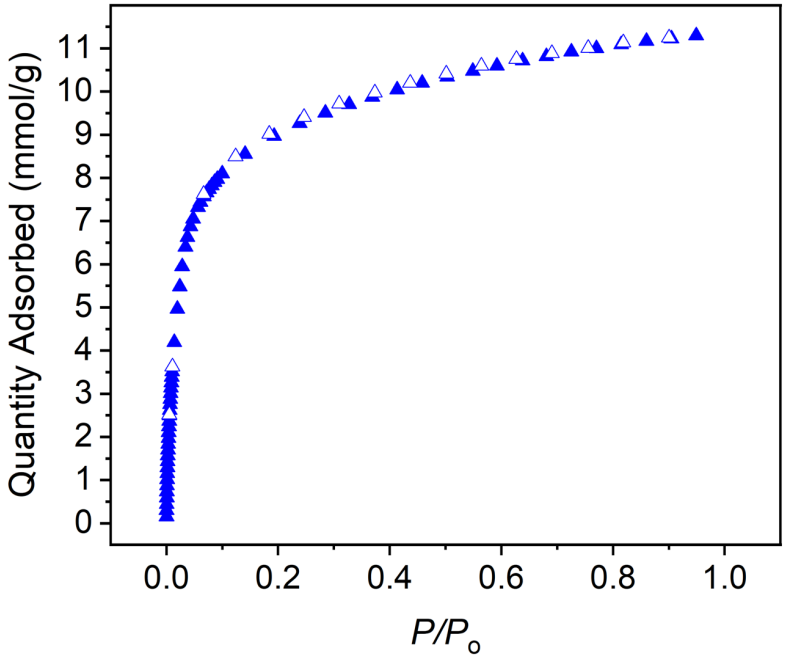

Figure S4.17. CO_2 adsorption (closed triangles) and desorption (open triangles) measured at 195 K for the DABCO-polymerized material.

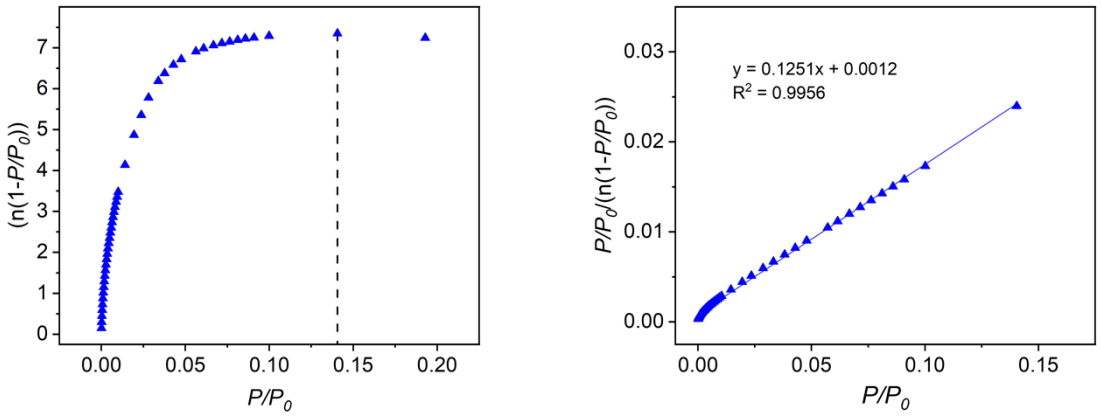

Figure S4.18. Left: Plot of n(1-P/P_0) vs. P/P_0 to determine the maximum P/P_0 used in the BET linear fit according to the first BET consistency criterion for CO_2 adsorption at 195 K for the DABCO polymerized cage. Right: The slope of the best fit line for $P/P_0 < 0.141$ is 0.1251 and the y-intercept is 0.0012, which satisfies the second BET consistency criterion. This results in a measured surface area of 818 m^2/g.

Comparison of Gas Uptake in Capped cages

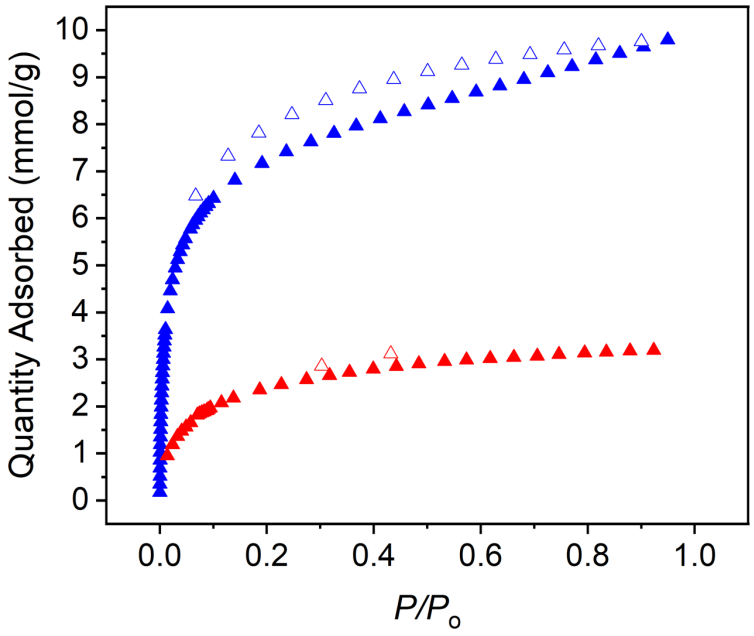

Figure S4.19. Comparison of 195 K CO_2 adsorption (closed triangles) and desorption (open triangles) isotherms for the H-esp cage activated under optimal conditions (blue) and when precipitated from DMA with MeOH (red).

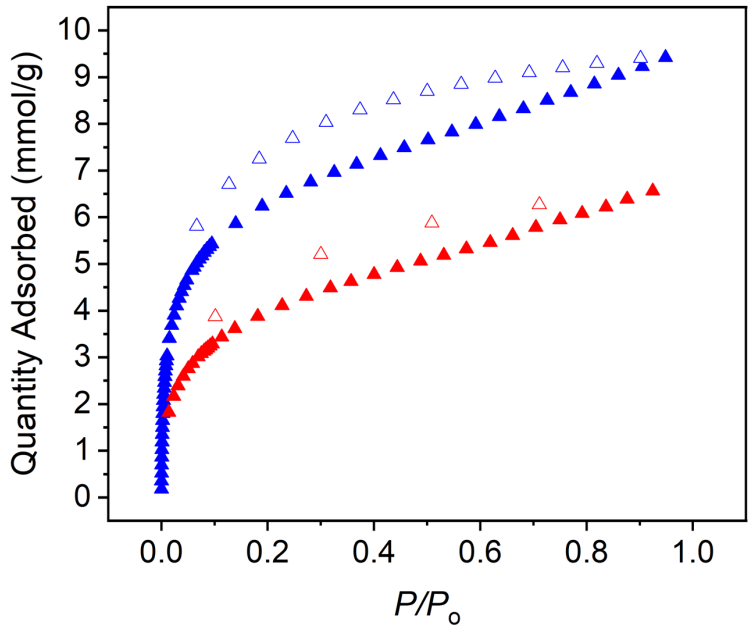

Figure S4.20. Comparison of 195 K CO_2 adsorption (closed triangles) and desorption (open triangles) isotherms for the ^{t}Bu-esp cage activated under optimal conditions (blue) and when precipitated from DMA with MeOH (red).

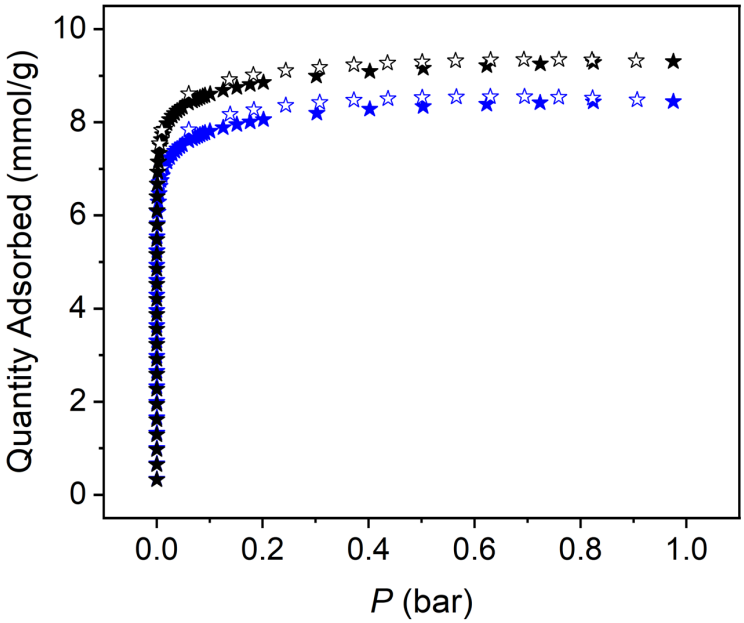

Figure S4.21. Comparison of 77 K N_2 adsorption (closed stars) and desorption (open stars) isotherms for the H-esp cage (black) and ^{t}Bu-esp cage (blue) activated under optimal conditions.

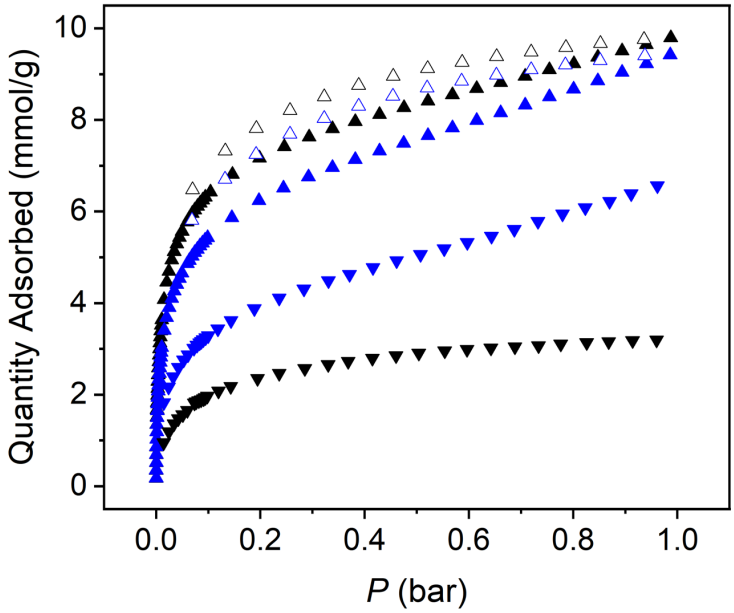

Figure S4.22. Comparison of 195 K CO_2 adsorption (closed triangles) and desorption (open triangles) isotherms for the H-esp cage (black) and ^{t}Bu-esp cage (blue) activated under optimal conditions (triangles) or when precipitated from DMA with methanol prior to solvent exchange (inverted triangles).

Comparison of esp-capped cage and DABCO polymer

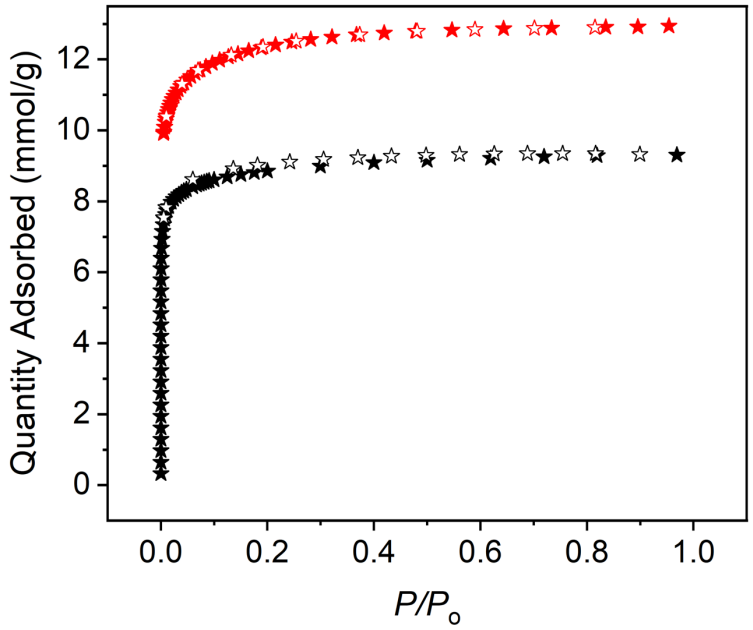

Figure S4.23. Comparison of 77 K N_2 adsorption (closed stars) and desorption (open stars) isotherms for the H-esp cage (black) and the DABCO polymerized material (red).

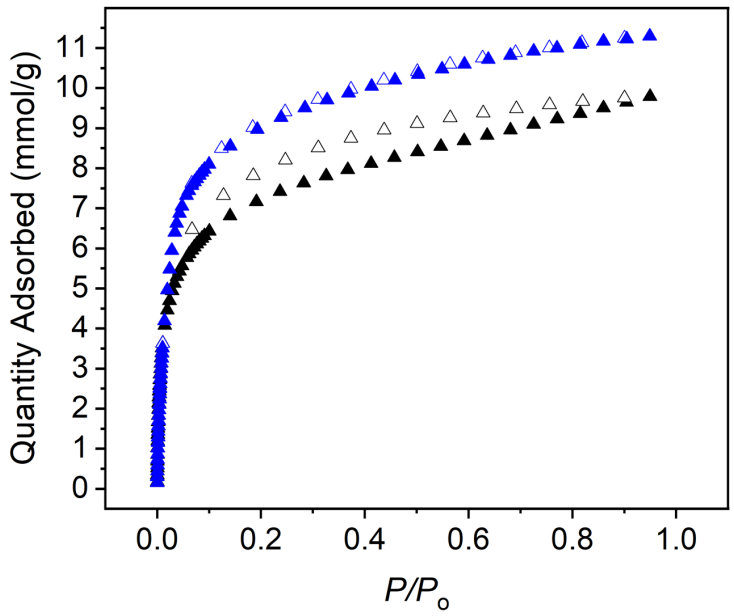

Figure S4.24. Comparison of 195 K CO_2 adsorption (closed triangles) and desorption (open triangles) isotherms for the H-esp cage (black) and the DABCO polymerized material (blue).

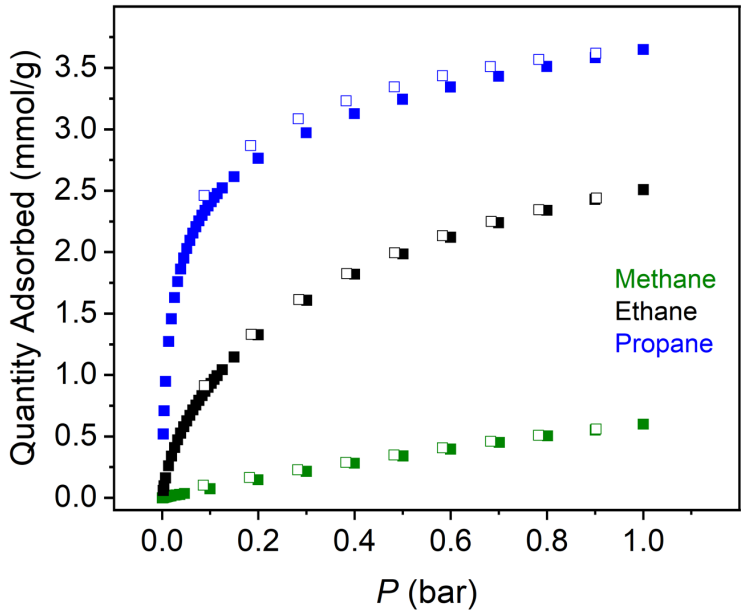

Figure S4.25. Low pressure hydrocarbon adsorption (closed squares) and desorption (open squeares) in the H-esp cage, $Mo_{12}(btc)_4(H\text{-}esp)_6$, measured at 298 K.

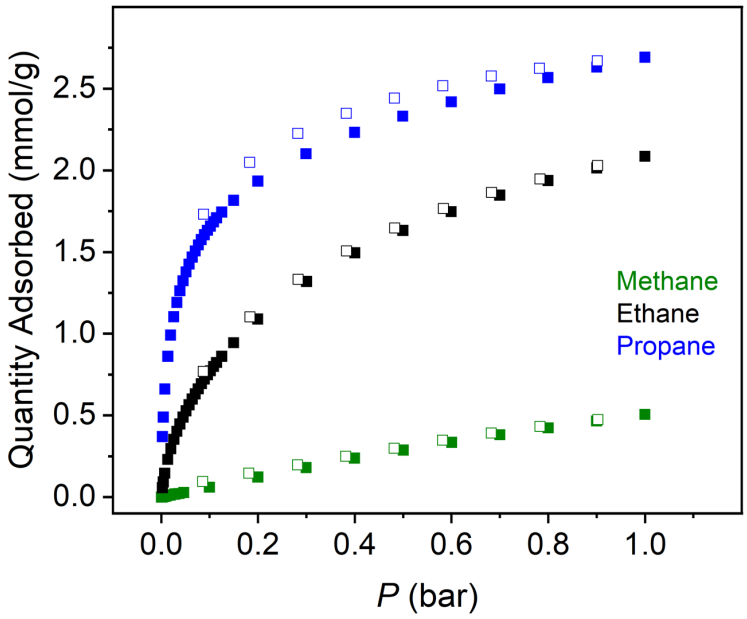

Figure S4.26. Low pressure hydrocarbon adsorption (closed squares) and desorption (open squares) in the ^{t}Bu-esp cage, $Mo_{12}(btc)_4(^t Bu\text{-}esp)_6$, measured at 298 K.

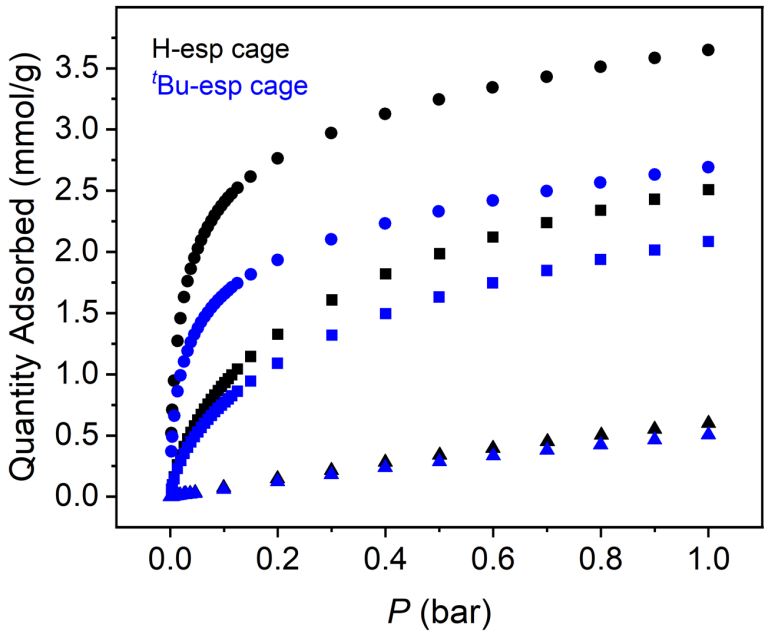

Figure S4.27. Comparison of 298 K low pressure methane (triangles), ethane (squares), and propane (circles) adsorption in the H-esp (black) and ^{t}Bu-esp (blue) cages.

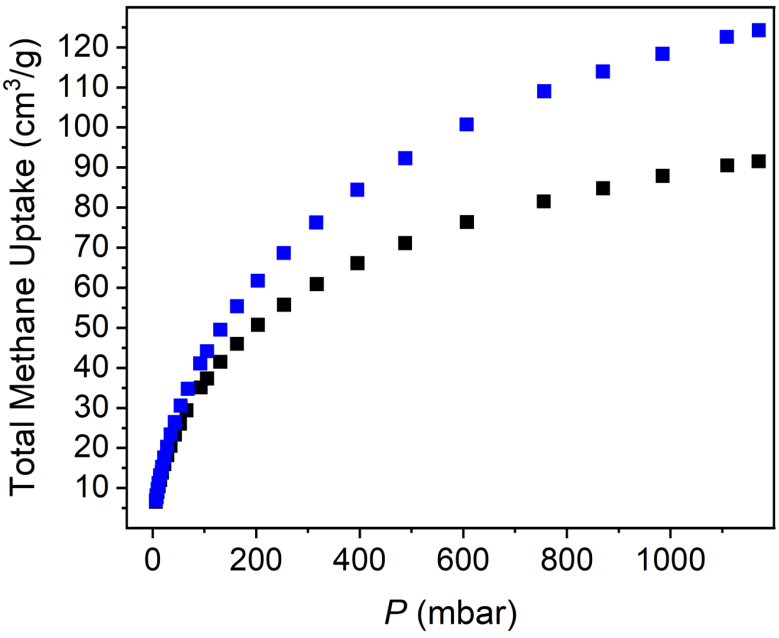

Figure S4.28. Comparison of low pressure, 195 K methane adsorption in the H-esp cage (black) and the DABCO-polymerized material (blue).

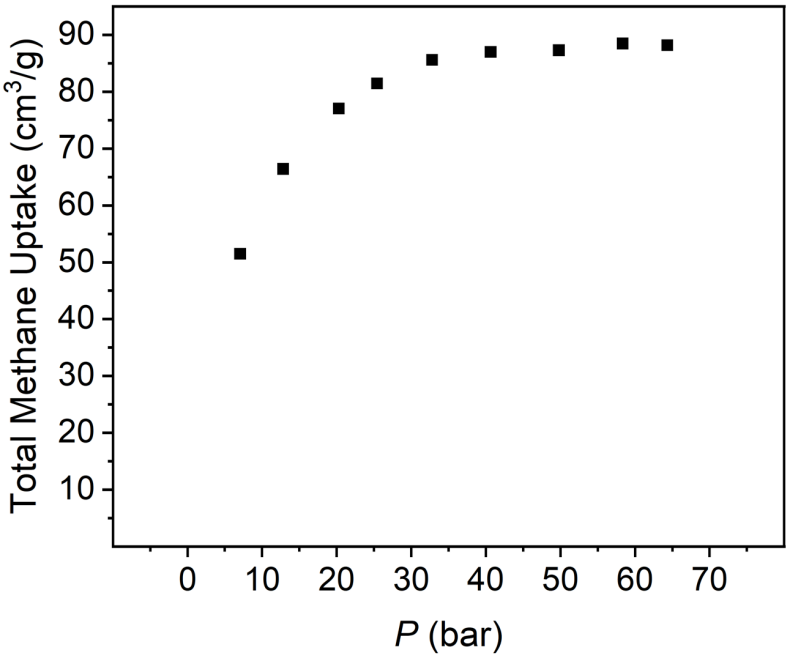

Figure S4.29. High pressure methane adsorption in the H-esp cage at 298 K.

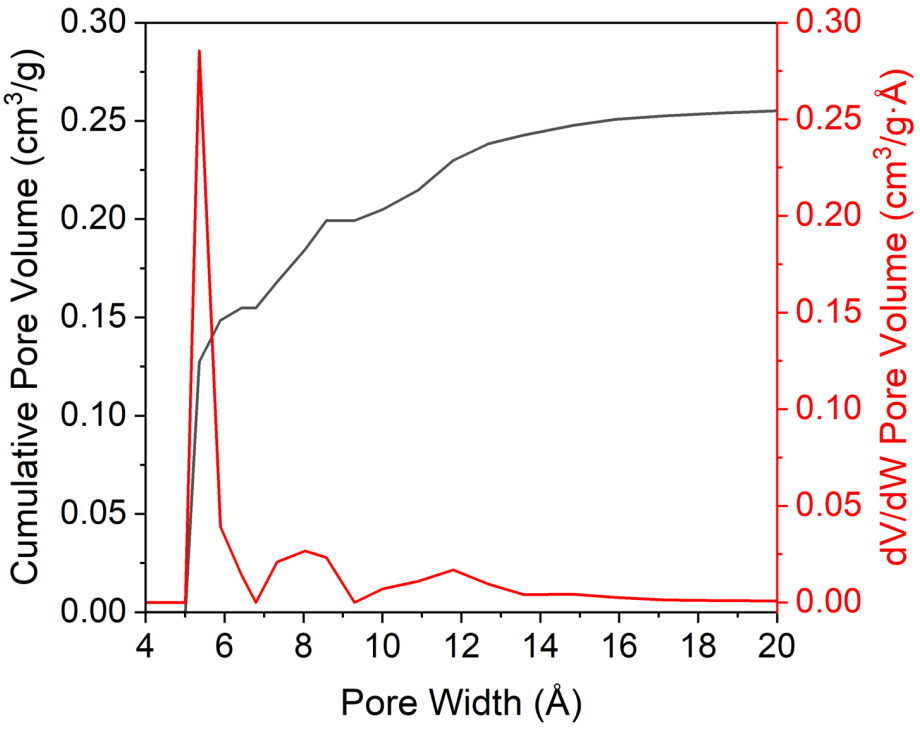

Figure S4.30. Pore size distribution in the H-esp cage calculated from N_2 adsorption at 77 K.

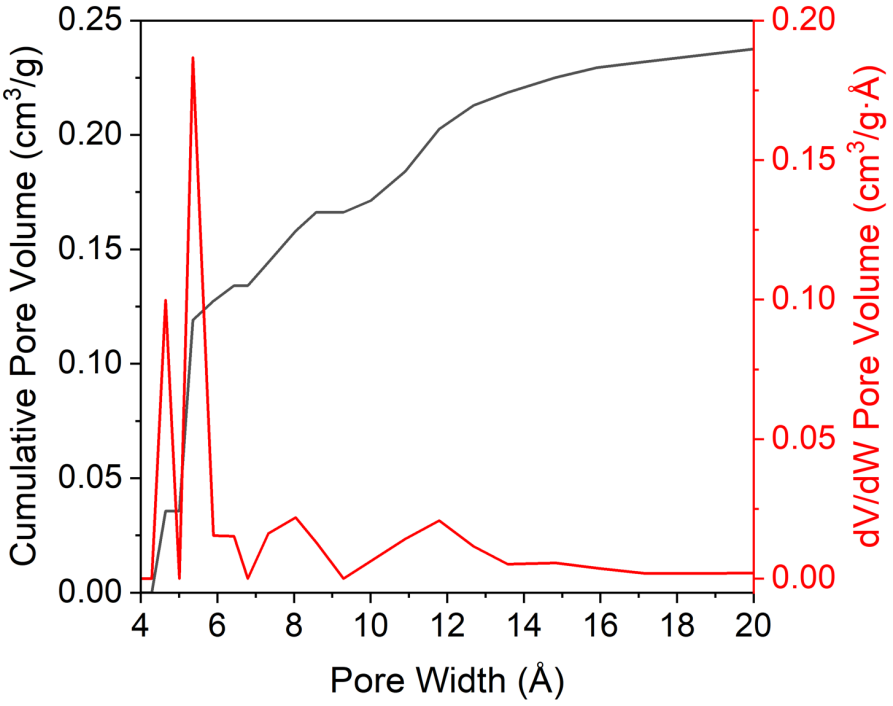

Figure S4.31. Pore size distribution in the ^{t}Bu-esp cage calculated from N_2 adsorption at 77 K.

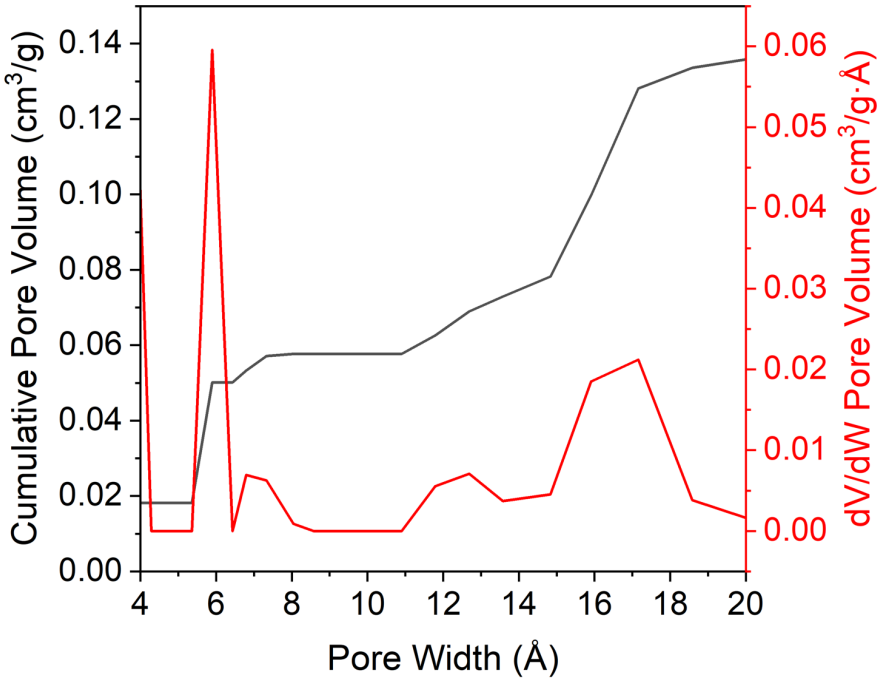

Figure S4.32. Pore size distribution in the previously reported MoDTolF cage calculated from N_2 adsorption at 77 K.

5. UV-Visible Spectra

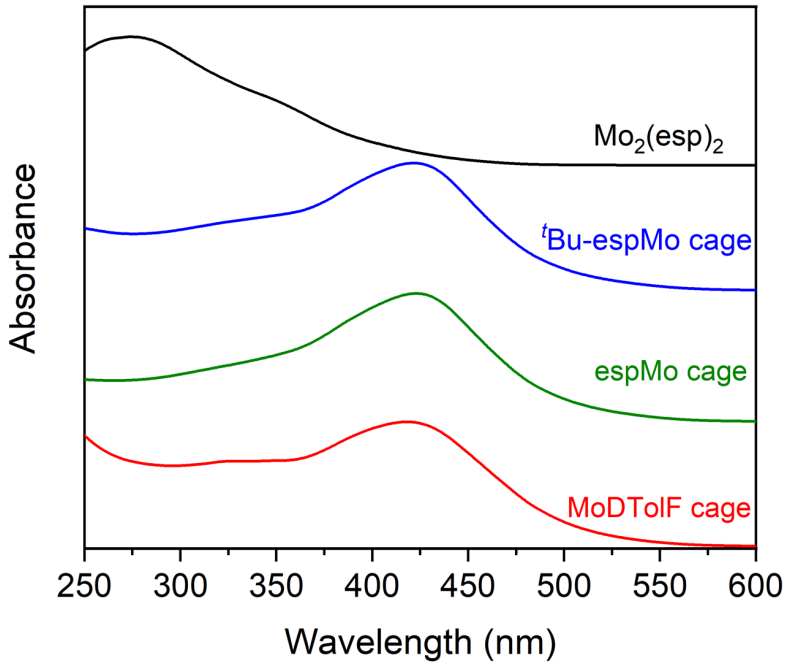

Figure S5.1. UV-visible spectra of the $Mo_2(esp)_2$ paddlewheel complex (black), the ^{t}Bu-esp Mo cage (blue), the esp Mo cage (green), and the previously reported MoDTolF cage (red) collected in pyridine.

6. Thermogravimetric Analysis

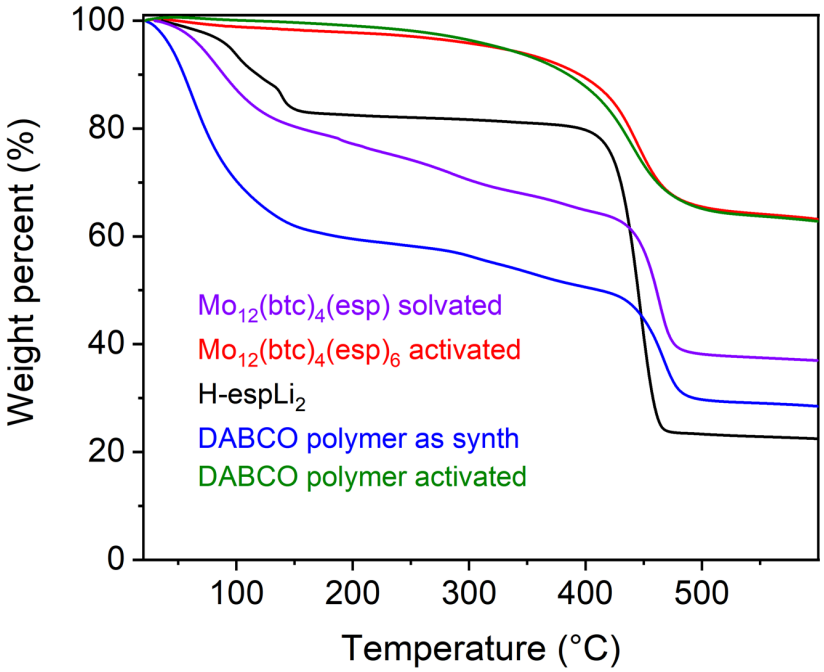

Figure S6.1. TGA plot of the solvated (purple) and activated $Mo_{12}(btc)_4(esp)_6$ cage (red), as well as H-$espLi_2$ (black), the as synthesized (blue) and activated DABCO polymer (green).

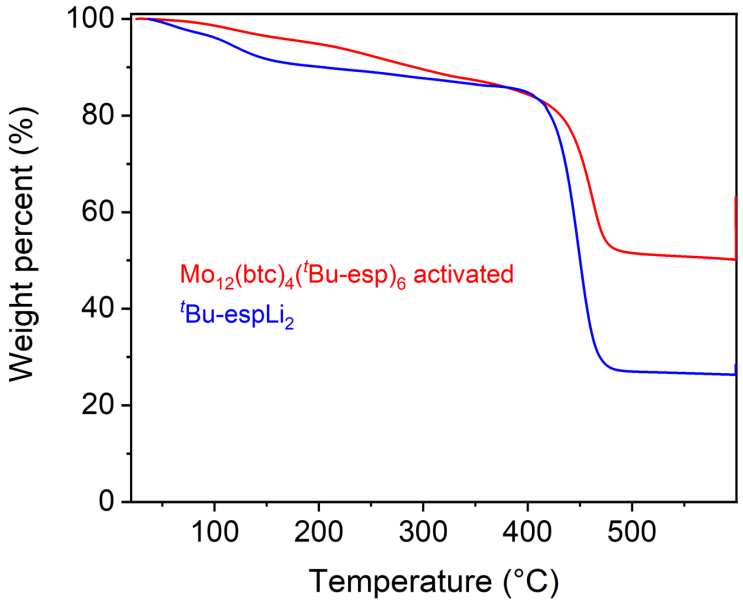

Figure S6.2. TGA plot of the activated $Mo_{12}(btc)_4(^t$Bu-$esp)_6$ cage (red) and ^{t}Bu-$espLi_2$ (black).

8. SEM Images

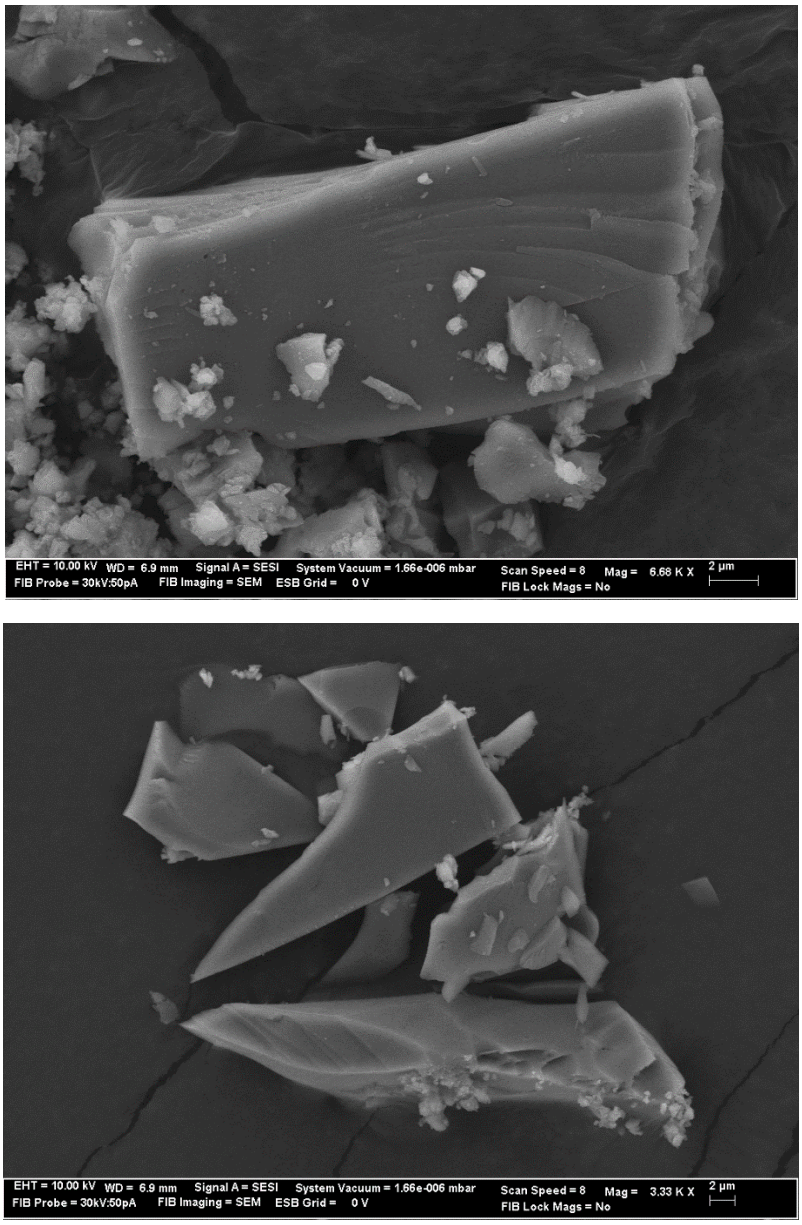

Figure S7.1. SEM images of the amorphous cage phase generated upon evaporation of a pyridine solution of cage.

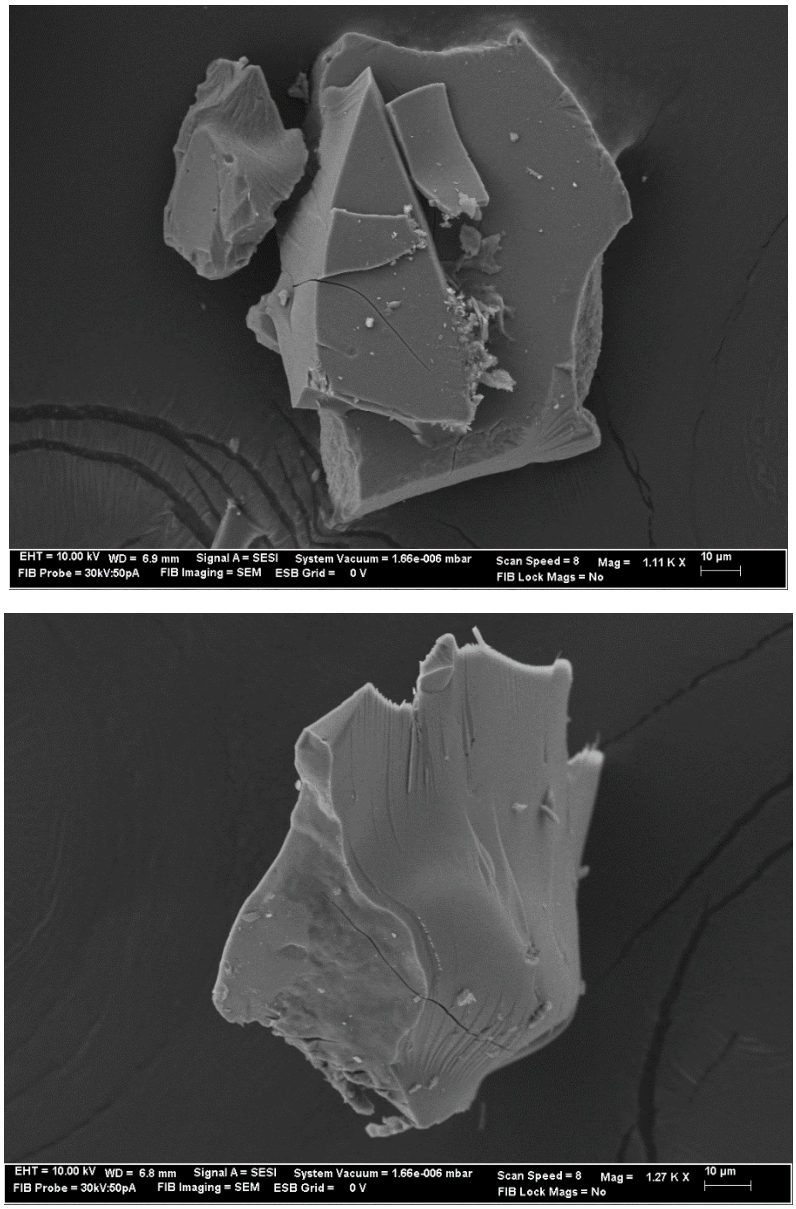

Figure S7.2. SEM images of the amorphous DABCO-linked polymer.